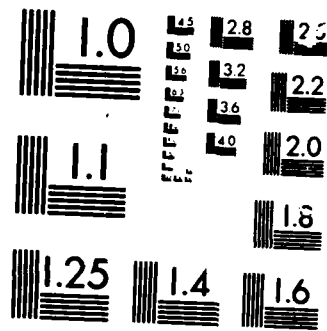CODA OBSERVED A NORSAR AND NORESS(U) GEORGIA TECH
RESEARCH INST ATLANTA A M DAINTY 20 AUG 85
AFGL-TR-85-0199 F19628-85-K-0019

UNCLASSIFIED

F/G 8/11   NL

	1.0		2.8	2.5
			3.2	
			3.6	2.2
	1.1		4.0	2.0
				1.8
	1.25	1.4	1.6

MICROCOPY RESOLUTION TEST CHART

AFGL-TR-85-0199

AD-A166 454

Coda Observed at NORSAR and NORESS

Anton Michael Dainty

Georgia Tech Research Institute
Atlanta, Georgia 30332

20 August 1985

Final Report
20 December 1984 – 30 June 1985

DTIC
ELECTE
APR 0 9 1986
E

OTIC FILE COPY

86   4   8   024

Sponsored By
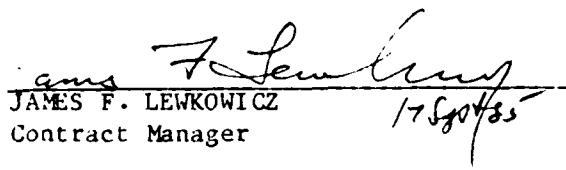
Defense Advanced Research Projects Agency (DoD)
Defense Sciences Office, Geophysical Sciences Division
DARPA/DSO Physical Characterization of Seismic Sources
ARPA Order No. 5299
Issued by the Air Force Geophysics Laboratory
under Contract No. F19628-85-K-0019

This technical report has been reviewed and is approved for publication.

JAMES F. LEWKOWICZ   /7 Sep 85   HENRY A. OSSING
Contract Manager   Chief, Solid Earth Geophysics Branch

FOR THE COMMANDER

DONALD H. ECKHARDT
Director
Earth Sciences Division

This report has been reviewed by the ESD Public Affairs Office (PA) and is releasable to the National Technical Information Service (NTIS).

Qualified requestors may obtain additional copies from the Defense Technical Information Center. All others should apply to the National Technical Information Service.

If your address has changed, or if you wish to be removed from the mailing list, or if the addressee is no longer employed by your organization, please notify AFGL/DAA, Hanscom AFB, MA 01731. This will assist us in maintaining a current mailing list.

6a. NAME OF PERFORMING ORGANIZATION	6b. OFFICE SYMBOL (If applicable)	7a. NAME OF MONITORING ORGANIZATION
Georgia Tech Research Institute		Air Force Geophysics Laboratory

6c. ADDRESS (City, State and ZIP Code)	7b. ADDRESS (City, State and ZIP Code)
Atlanta, Georgia 30332	Hanscom AFB Massachusetts 01731-5000

8a. NAME OF FUNDING/SPONSORING ORGANIZATION	8b. OFFICE SYMBOL (If applicable)	9. PROCUREMENT INSTRUMENT IDENTIFICATION NUMBER
Air Force Geophysics Laboratory		F19628-85-K-0019

8c. ADDRESS (City, State and ZIP Code)	10. SOURCE OF FUNDING NOS.			
	PROGRAM ELEMENT NO.	PROJECT NO.	TASK NO.	WORK UNIT NO.
Hanscom AFB Massachusetts 01731				
11. TITLE (Include Security Classification) Coda Observed at NORSAR and NORESS (unclassified)	61101E	1795	5A10DA	5A10DAAP

12. PERSONAL AUTHOR(S)
DAINTY, ANTON MICHAEL

13a. TYPE OF REPORT	13b. TIME COVERED	14. DATE OF REPORT (Yr., Mo., Day)	15. PAGE COUNT
Final	FROM 12/20/84 TO 6/30/85	1985 August 20	80

16. SUPPLEMENTARY NOTATION

17. COSATI CODES			18. SUBJECT TERMS (Continue on reverse if necessary and identify by block number)
FIELD	GROUP	SUB. GR.	Teleseismic Coda NORSAR NORESS f-k

19. ABSTRACT (Continue on reverse if necessary and identify by block number)

The purpose of this study was to determine the nature of the teleseismic P coda seen on short period seismograms, and specifically to separate it into a contribution from scattering near the source, if the source is in the crust, and scattering near the receiver. To accomplish this, digital data from NORSAR and NORESS were used in the frequency range 1-7 Hz and covering a time span of 20-200 sec after first P. The variation of the coda power spectrum of various types of events with time was examined and found to fit a simple exponential decay for all events, although the amplitude of the coda relative to first ‹P was quite different for different types of events, being large for crustal earthquakes and lower for deep focus earthquakes and explosions. Data from NORESS were examined using frequency-wavenumber methods, particularly by

(Continued on reverse)

19. ABSTRACT (Continued)

determining the power as a function of wavenumber at a fixed frequency; this is equivalent to finding the power as a function of apparent velocity. Deep focus events had a coda dominated by low apparent velocities (3.5-4.5 km/sec), explosions a coda with equal power in high (10 km/sec) and low apparent velocities, crustal earthquakes a coda dominated by high apparent velocities. These results indicate that the teleseismic P coda in the time and frequency considered indeed consists of energy scattered near the source if the source is in the crust (the high apparent velocity component), and energy scattered near the receiver (low apparent velocity component). The low velocities indicate that teleseismic P to Lg (trapped shear wave) is the dominant mode of scattering near the receiver; the differences between crustal earthquakes and explosions suggest Lg to teleseismic P near the source. Multiple scattering is probably occurring in the coda. These results indicate that coda magnitudes will depend on conditions in broad (∿500 km) regions around the source and receiver, perhaps explaining their stability. It may be possible to separate the coda from the source and receiver regions, leading to even greater stability. The difference between crustal earthquakes and explosions may be useful as a discriminant.

Accession For

NTIS GRA&I

DTIC TAB

Unannounced

Justification

By

Distribution/

Availability Codes

Dist | Avail and/or Special

A-1

TABLE OF CONTENTS

LIST OF FIGURES

LIST OF TABLES

ABSTRACT

The purpose of this study was to determine the nature of the tele-
seismic P coda seen on short period seismograms, and specifically to
separate it into a contribution from scattering near the source, if the
source is in the crust, and scattering near the receiver. To accomplish
this, digital data from NORSAR and NORESS were used in the frequency
range 1-7 Hz and covering a time span of 20-200 sec after first P. The
variation of the coda power spectrum of various types of events with
time was examined and found to fit a simple exponential decay for all
events, although the amplitude of the coda relative to first P was quite
different for different types of events, being large for crustal earth-
quakes and lower for deep focus earthquakes and explosions. Data from
NORESS were examined using frequency-wavenumber methods, particularly by
determining the power as a function of wavenumber at a fixed frequency;
this is equivalent to finding the power as a function of apparent velo-
city. Deep focus events had a coda dominated by low apparent velocities
(3.5-4.5 km/sec), explosions a coda with equal power in high (10 km/sec)
and low apparent velocities, crustal earthquakes a coda dominated by
high apparent velocities. These results indicate that the teleseismic P
coda in the time and frequency range considered indeed consists of energy
scattered near the source if the source is in the crust (the high apparent
velocity component), and energy scattered near the receiver (low apparent
velocity component). The low velocities indicate that teleseismic P to
Lg (trapped shear wave) is the dominant mode of scattering near the
receiver; the differences between crustal earthquakes and explosions

suggest Lg to teleseismic P near the source. Multiple scattering is probably occurring in the coda. These results indicate that coda magnitudes will depend on conditions in broad (~500 km) regions around the source and receiver, perhaps explaining their stability. It may be possible to separate the coda from the source and receiver regions, leading to even greater stabilty. The difference between crustal earthquakes and explosions may be useful as a discriminant.

INTRODUCTION AND PREVIOUS WORK

Coda waves are waves seen on a seismogram after the arrival of the phases expected due to propagation in a spherically symmetric earth. These waves are not readily explainable in terms of deterministic paths, and accordingly it is felt they are randomly scattered waves (Aki, 1969). The phenomenon is ubiquitous, especially at high frequencies, being found at local, regional, and teleseismic ranges, for shallow and deep focus events and for earthquakes and explosions. Coda has been used as a magnitude estimator for nuclear explosions (Bullitt and Cormier, 1984; Baumgardt, 1983; Ringdal, 1983), and seems to be a more stable estimator than other methods. The purpose of this study is to examine coda waves from 1 to 10 Hz of teleseismic events using NORSAR and the new facilities at the NORESS regional seismic array near Oslo, Norway (Mykkeltveit and Bungum, 1984).

Previous work on codas can be divided into analytical and qualitative. Analytical work has tended to focus on the quantitative characterisation of the power level as a function of frequency and time (Aki, 1969; Aki and Chouet, 1975; Dainty et al., 1984), while qualitative work has turned to find the nature and source of scattered waves (Greenfield, 1971; King et al., 1975), although some quantitative work was done in both of the papers referenced. The (rather simple) analytical theory is applicable to data taken at a single seismometer. The more qualitative approaches have used array data, allowing a separation of the wave field by azimuth and phase velocity. Very recently, work has also been done using three-component data.

In this study an attempt is made to combine the analytical and qualitative features of previous studies. Data from two subarrays at NORSAR are examined using a theory similar to that of Aki and Chouet (1975) applied to the individual seismometers; the results (coda Q and side-scattering turbidity) are then averaged. Three sets of data are examined in this phase: a set of Semipalatinsk explosions, a set of Nevada Test Site explosions, and a set of deep focus earthquakes from the Bonin-Japan-Kurile subduction zone. In addition, some limited data from NORESS is analysed by this technique, including three large Semipalatinsk explosions, three shallow earthquakes, two deep focus earthquakes from the Bonin Trench, and an intermediate depth earthquake from the Hindu Kush.

The events recorded at NORESS are also analysed by frequency-wavenumber techniques using an analysis package developed by D. B. Harris of Livermore National Laboratory. Specifically, I have found the power as a function of wavenumber, or phase velocity, at a given frequency--this may be used to gain a quantitative picture of the partition of energy between different wave types and scattering regions.

The overall goal of the study was to determine what type of waves (P, S, or surface) are present in the coda, and where the scattering occurs. These are crucial basic questions that must be answered for evaluation of the use of coda as a magnitude estimator.

MODELS, THEORETICAL DEVELOPMENT, AND TESTS

Models

Two models are important in considering the coda: a model of those
features of the earth that are supposed to produce the coda and the
resulting model of the coda in terms of seismic waves. The model of the
earth adopted for coda purposes is shown in Figure 1. Inhomogeneities
("point scatterers") are randomly distributed throughout the crust only.
The distribution of scatterers is considered to be laterally quasi-
stationary; i.e., in a given broad region (e.g., Norway, East Kazakh)
the statistical properties of the scatterers does not vary laterally.
The properties may be different between regions, however; the appro-
priate definition of a region shall be discussed below. The distribu-
tion of scatterers is considered to vary vertically with depth, since
the scatterers are confined to the crust. The scatterers may be charac-
terized either by a number density and a cross-section (Dainty et al.,
1984) or by turbidity, which may be regarded as the cross-section per
unit volume. Scattered intensity depends on the scattering angle and
frequency, according to the size, shape, and elastic characteristics of
the scatterers; in this report scattering angles less than 90° will be
described as forward scattering; greater than 90°, backscattering; and
near 90° as side scattering.

The theory used to translate the earth model into a model of
seismic waves in the coda is the single scattering, independent scat-
terers model as used by Aki and Chouet (1975). From Figure 1, we see
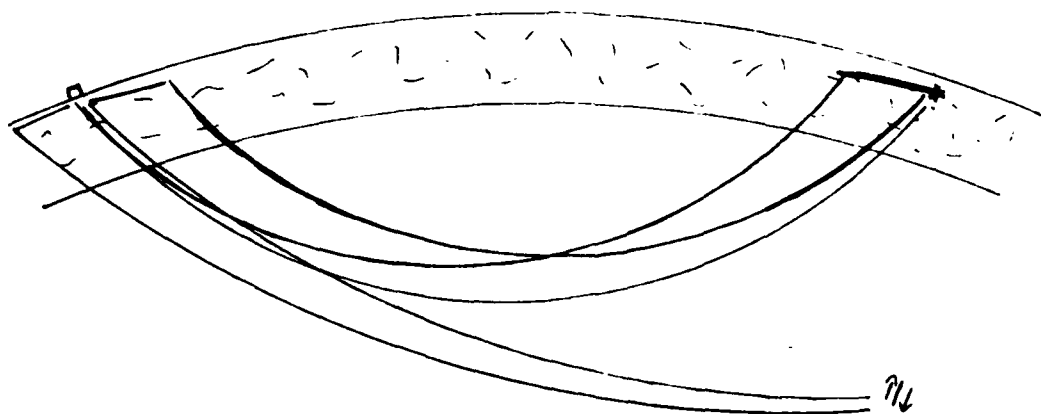that all scattering will occur in the lithosphere "near" either the

Figure 1. Earth model and typical ray paths for direct P and coda arrivals for a near surface explosion and a deep focus earthquake.

source or the receiver, with travel as a P wave between (see below).

For local events, the appropriate theory is given in Dainty et al.

(1984) leading to equations 12 and 14 in that work for the coda power

spectrum as a function of time. For the purposes of this report, we

note that this theory predicts that certainly for times greater than

twice the S wave travel time the coda waves will be backscattered and

will have traveled from a scatterer at a distance $d \approx \frac{\nu t}{2}$, where ν is

the wave velocity (3.5 to 8 km/sec) and t is time after origin. Since

t ˙ 100 sec in this sduty, $d \sim 150 \rightarrow 500$ km; i.e., "near" for the

purposes of this study is a few hundred kilometers. The local coda

theory can be written in terms of either cylindrical or spherical

spreading; results quoted in Dainty et al. (1984) tend to support

cylindrical spreading. Since the waves are backscattered, P to S and S

to P conversions should not be important (Wu, 1984).

Theoretical Development

For telese smic P codas, two problems will be discussed here--

namely, the production of coda near the receiver and near the source.

Only the case of production of coda near the source by primary waves

will be discussed in detail, for the case where the outgoing waves are

vertical. From Figure 2, we note that a variety of scattered waves are

possible. However, since P and S waves travel the 50 km through the

crust in 10 to 15 sec, coda waves delayed for significantly longer times

than this after first P onset have traveled nearly horizontally before

being scattered at about 90° (side scattering). We shall present a

detailed theory for scattering of trapped shear waves (Lg) into

(a)

(b)
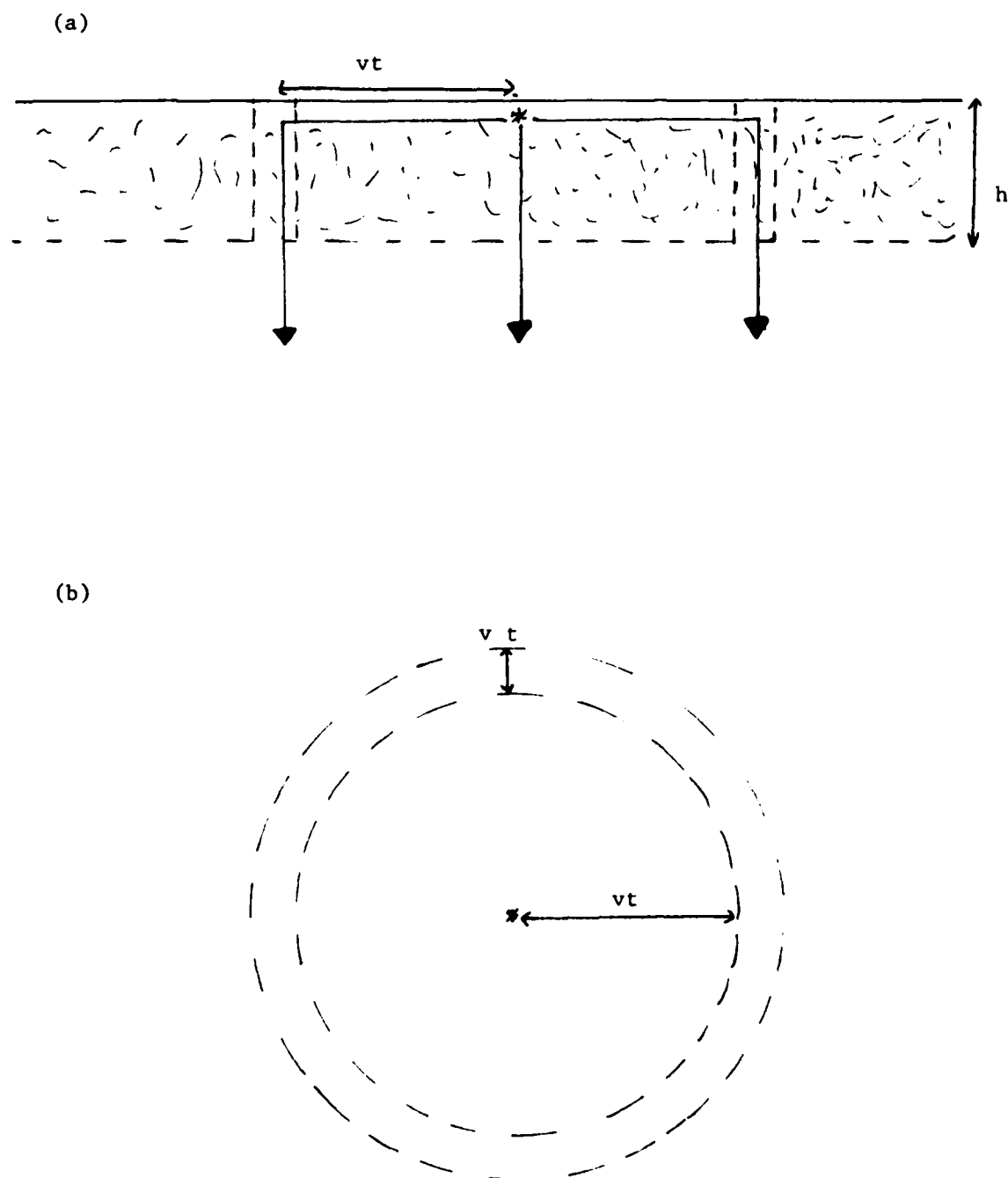
Figure 2. Geometry for near source scattering. (a) Section view.
(b) Map view.

teleseismic P waves and quote formulas for other cases. From Figure 2, note that at time t to $t + \Delta t$ after origin the primary Lg wave will encounter scatterers at a range vt to $v(t + \Delta t)$, where v is the Lg wave velocity. The amplitude of the primary wave, assumed to be a short wavelet of dominant frequency f, will be

$$A(f,t) = A_L(f) \frac{1}{\sqrt{vt}} \exp(-\pi ft/Q) \tag{1}$$

Q in (1) is the total Q as discussed in Dainty et al. (1984). Under the theory of independent scatterers, the squared amplitudes of the scattered waves arriving between t and $t + \Delta t$ are added on the grounds that the arrivals are incoherent. If it is assumed that the travel time in all mantle paths is approximately equal in Figure 1, then t in (1) may be interpreted as the lapse time after first P onset, and the sum at a unit distance from the surface, for waves scattered vertically downwards from ΔV, is

$$A_s^2 = A^2 \cdot \Delta V \cdot g_{LPS} \tag{2}$$

where g_{LPS} is the side scattering turbidity for Lg to P conversion. From Figure 2,

$$\begin{aligned} \Delta V &= 2\pi(vt)h \cdot \Delta(vt) \\ &= 2\pi v^2 th \cdot \Delta t \end{aligned} \tag{3}$$

where h is the thickness of the scattering layer (crust). Using (1), (2), and (3),

$$A_s^2 = A_L^2(f) \cdot 2\pi vh \cdot g_{LPS} \cdot \exp[-2\pi ft/Q] \cdot \Delta t \tag{4}$$

and

$$A_s^2 = P_c(f,t) \triangle t \tag{5}$$

where $P_c(f,t)$ is the coda power spectrum as a function of time (Aki and Chouet, 1975). Accordingly, at unit distance from the surface, the coda power spectrum due to surface wave to P scattering is

$$P_c(f,t) = A_p^2(F) \cdot 2\pi\nu \cdot g'_{LPS} \cdot \exp[-2\pi f t/Q] \tag{6}$$

where $A_p(f)$ is the amplitude of the direct P arrival, t is now time after P onset, and the apparent side scattering turbidity is given by

$$g'_{LPS} = \frac{A_L^2}{A_{po}^2} \cdot h \cdot g_{LPS} \tag{7}$$

If we assume that the P wave and the coda have the same amplitude dependance with distance in the mantle (Figure 1), (6) will also hold at a teleseismic station. In (7), however, A_L and A_{po} are considered measured at unit distance from the source, and hence "o" has been added to the p subscript.

A similar analysis may be made for Lg scattered into the receiver from a plane P wave striking the surface near the receiver. The coda power spectrum is given by

$$P_c(f,t) = A_p^2(f)g''_{PLS} \cdot 2\pi\nu \cdot \exp[-2\pi f t/Q] \tag{8}$$

with

$$g''_{PLS} = g_{PLS} \cdot h \tag{9}$$

Formulas may also be quoted for side scattered body waves near the
receiver and near the source--all formulas have the form

$$P_c(f,t) = A_p^2 \, g'_{xys} \cdot \frac{2\pi}{t} \cdot \exp[-2\pi ft/Q] \qquad (10)$$

where

$$g'_{xys} = h \cdot g_{xys} \qquad (11)$$

For scattering near the source, y is P and x can be P or S. For
scattering near the receiver, x is P and y can be P or S. Similar
arguments to that given for local events show that "near" is within a
few hundred kilometers.

To apply this theory, write for the power spectrum of the coda, for
an event in the crust,

$$(P_c)_{total} = (P_c)_{source} + (P_c)_{receiver} + (P_c)_{cross} + (P_c)_{other} \qquad (12)$$

In (12), the total coda power is considered to be the sum of coda from
the source that travels directly to the receiver along ray paths in the
mantle close to the first P onset, coda generated near the receiver by
the direct P wave, coda generated near the receiver by coda generated
near the source and travelling to the receiver along mantle P paths
("cross-coda"), and coda due to other sources such as PP (King et al.,
1975). As a first attempt, the last two terms in (12) will be
neglected, giving, for the Lg case,

$$(P_c)_{total} = (P_c)_{source} + (P_c)_{receiver} \qquad (13)$$

Using (6) and (8) for $(P_c)_{source}$ and $(P_c)_{receiver}$,

$$(P_c)_{total} = 2\pi A_p^2(f) \cdot [g'_{LPS} \exp(-2\pi ft/Q_s) \cdot \nu_s$$
$$+ g''_{PLS} \exp(-2\pi ft/Q_r) \cdot \nu_r] \qquad (14)$$

In (14), ν_s and Q_s are ν and Q at the source, ν_r and Q_r at the receiver. If these quantities are not too dissimilar, they may be replaced by their averages $\bar{\nu}$ and $\bar{Q}$. Then

$$(P_c)_{total} = 2\pi A_p^2(f)\bar{\nu} \cdot \exp[-2\pi ft/\bar{Q}] \cdot G \qquad (15)$$

where

$$G = g'_{LPS} + g''_{PLS}$$
$$= h_s \cdot g_{LPS} \cdot \frac{A_L^2}{A_{po}^2} + h_r \, g_{PLS} \qquad (16)$$

using (7) and (9); h_s and h_r are the crustal thickness at source and receiver, respectively. If P or S body waves to teleseismic P scattering is assumed, then

$$(P_c)_{total} = A_p^2(f) \cdot \frac{2\bar{\nu}}{t} \cdot \exp[-2\pi ft/\bar{Q}] \cdot G' \qquad (17)$$

with an equivalent formula to (16) for G'. G and G' will be called "effective side scattering turbidities" in this report.

Test of the Model

The model proposed has two essential features, one subsidiary feature, and one important unknown. The two essential features are: the scattering that produces the coda occurs in the crust near the source (for a source in the crust) and near the receiver; the energy in

the coda travels as unscattered P in the mantle along paths similar to the direct P onset. Thus the question of <u>where</u> scattering occurs is important. A subsidiary feature is the use of single incoherent scattering theory to derive relations such as (15)--this is considered subsidiary because if it were not true, the theory would have to be redone, but with in the same overall framework. The important unknown is <u>what types</u> of wave are involved in the scattering. Near the source the scattering is from an unknown wave type to teleseismic P, near the receiver from teleseismic P to an unknown wave type.

Some questions can be dealt with by a careful choice of data. The events used in this study are all at teleseismic distances, between 40° and 80° from NORSAR. P-wave travel times are at least 9 minutes for first P onset and at least 15 minutes for first S onset. Using a time span of 20-200 sec after first P in the coda effectively eliminates any travel path involving substantial S propagation in the mantle. There are also not many classical seismological phases that might contribute to the coda--PP, PcP, and (for the deep focus events) the depth phases pP and sP. The lower limit of time (20 sec after P onset) ensures the assumption of side scattering used in the theory section is justified. This point will be discussed further in the section on <u>Results</u>.

How may the remaining questions be answered using data available from NORSAR and NORESS? In this study, three techniques have been used. Using digital data from both the NORSAR and NORESS, equation (15) or (17) may be fitted to time series from individual seismometers to find values of G (or G') and $\overline{Q}$. This is a strategy similar to that employed by Aki (1980) or Dainty et al. (1984) for local events. It is

known from these and other investigations using this technique, however, that only very limited tests of the model may be carried out. Because of the simplification of (14) to produce (15), all information concerning <u>where</u> the energy is scattered is lost, except for one possibility to be discussed later. Information on <u>what</u> <u>types</u> of waves are involved is limited to comparisons of fits using (15) and (17), although some information may be obtained from this, c.f., Dainty <u>et</u> <u>al.</u> (1984), who suggest that Lg type waves are important in the local coda on this basis. The most pertinent use of this technique is to give a rough test of the model by seeing if the two independent parameter (G or G' and $\overline{Q}$) models of (15) and (17) do, in fact, fit the data, and to test for single or multiple scattering using two tests proposed by Dainty <u>et</u> <u>al.</u> (1984). These tests involve calculating an apparent total turbidity as

$$G_a = 2\pi f/(\overline{Q\nu}) \tag{18}$$

This is the total turbidity for the case of all attenuation due to single scattering, and is an upper bound for the true total turbidity. Then, for the theory to be valid, certainly

$$G,G' < G_a \tag{19}$$

Another condition suggested by Sato (1977) states that single scattering will be dominant if the maximum lapse time after first P onset t_{max} obeys

$$t_{max} < 1/(G_a \overline{\nu}) \tag{20}$$

Relation (19) is necessary but not sufficient; (20) is sufficient but
may not be necessary (see Dainty and Toksöz, 1981).

The second analysis method is to use the NORESS array to determine
the azimuth and phase velocity (apparent velocity) of energy in the
coda. The NORESS array is well suited to this task, as discussed in the
next section. From Figures 1 and 2 and equation (14), the coda energy
arriving at the seismometer consists of two parts, a part coming from
the source azimuth as P waves at a small angle of incidence to the
vertical, and a part coming from the local scattering in the crust. The
part coming from the local scattering would be expected to have a
variety of azimuths, and to consist of crustal waves travelling near
horizontally in a medium with a P wave velocity of 6-8 km/sec and a
shear wave velocity of 3.5-4.5 km/sec. The phase, or apparent velocity
of a wave, detected by frequency-wavenumber (f-k) analysis at an array
is related to the near-surface medium velocity V_o (P or S as
appropriate) by

$$V_{phase} = V_o/\sin(i) \tag{21}$$

where i is the angle of incidence to the vertical. For the events
studied here, P waves coming from the source region have apparent
velocities of 13-22 km/sec (i = 15°-30°, assuming a near surface
velocity of 6 km/sec). P waves scattered near horizontally would have
phase velocities near 6 km/sec, S waves near 3.5 km/sec, and trapped
shear waves (Lg) 3.5-4.5 km/sec. Thus a determination of the azimuth
and, especially, the phase velocity of waves in the coda using the
NORESS array should partially answer the questions where and what type,

by allowing a separation into energy scattered at teleseismic distances and energy scattered near the array. The choice of a window starting 20 sec (or longer) after first P should eliminate forward scattered energy in the crust near the array, a necessary step since such energy would have high phase velocity. Multiple scattering, however, might produce high phase velocities due to energy scattered directly below the array.

However, the analyses so far proposed do not place many constraints on any high phase velocity part of the coda, which might have been scattered in the crust near the source (if the source is in the crust) or in the mantle or in some other path, such as PP. Indeed, it is known that PP contributes to the coda, from previous studies (King et al., 1975). To try and elucidate the nature of this portion of the coda, events of different types (crustal earthquakes and nuclear explosions) and different focal depths (shallow and deep) will be examined using both analysis techniques. According to the model shown in Figure 1, there should be no coda produced near the source for a deep focus event since the event is not in the (scattering) crust, but only coda produced near the receiver. There are two ways this might be detected. The value of G (or G') found from fitting (15) to data should be less for a deep focus event than for a crustal event, since the first term on the right in (16) is zero ($A_L = 0$). Since the coda from a deep focus event should consist solely of waves scattered in the crust near the receiver, only low phase velocities (6 km/sec (P), 3.5 km/sec (S), or 3.5-4.5 km/sec (Lg)) should be detected in the coda. For crustal events, high

phase velocity components from near-source scattering will also be present. This will help answer the question of _where_ near source (or mantle) scattering occurs. If these predictions concerning deep and shallow focus are confirmed, then some indication of the type of wave that is scattered near the source may be obtained by comparing crustal earthquakes with crustal explosions. Crustal earthquakes produce strong S and Lg; crustal explosions, strong P. If one or other of these source types produces a stronger coda, measured either through G or through the phase velocity spectrum, this will show what type of energy is scattered near the source.

In summary, _where_ the energy is scattered may be investigated using the NORESS array to determine phase velocity and events at different focal depths; _what_ _type_ of energy is involved may be investigated by phase velocity analysis at NORESS and the comparison of crustal earthquakes and explosions. Single or multiple scattering may be partially investigated by using the coda spectrum as a function of time and equation (15).

DATA AND ANALYSIS METHODS

Data

Four groups of events have been analysed; locations are shown on
Figure 3. The first three groups are events recorded at NORSAR, which
has been in operation since 1970 and hence allows a selection from a
considerable body of data. Criteria for selection were no clipping of
first P on the majority of seismometers of at least one of the two
subarrays (02B and 03C) selected, and as high a signal-to-noise ratio in
the coda as possible. The standard digitisation rate of 20 samples/sec
was observed for all seismograms, and 250 sec of data was taken, with at
least 30 sec of noise before first P onset included, leaving about 200
sec of seismogram for analysis. The last group consists of events
recorded at the NORESS array, sampled at 40 Hz. Generally, 120 sec of
record is used (but in some cases only 100 sec) with 15-20 sec of noise
before first P onset.

Table 1 gives details of deep focus events recorded at NORSAR from
the Japan-Bonin and Kamchatka-Kurile subduction zones, and Figure 4
shows an example of one of them. Table 2 describes events recorded at
NORSAR from the area of the Soviet test site near Semipalatinsk, East
Kazakhstan. With one exception (1976, March 20) these events are
presumed nuclear tests. Figure 5 is a map of the region with the
epicenters marked; the presumed tests seem to lie in three general
areas, called Shagan, Degelen SE, and Degelen NW in this report. Figure
6 shows an example of one of the presumed explosions. Table 3 tabulates
announced explosions at the Nevada Test Site recorded at NORSAR.

Figure 3. Location of events relative to NORSAR and NORESS (cross). Open circles are locations of events in this study. Numbers beside circles are epicenters at that (approximate) location, if different from 1.

Table 1. Deep focus events from the Japan-Bonin and Kamchatka-Kurile
subduction zones, recorded at NORSAR.

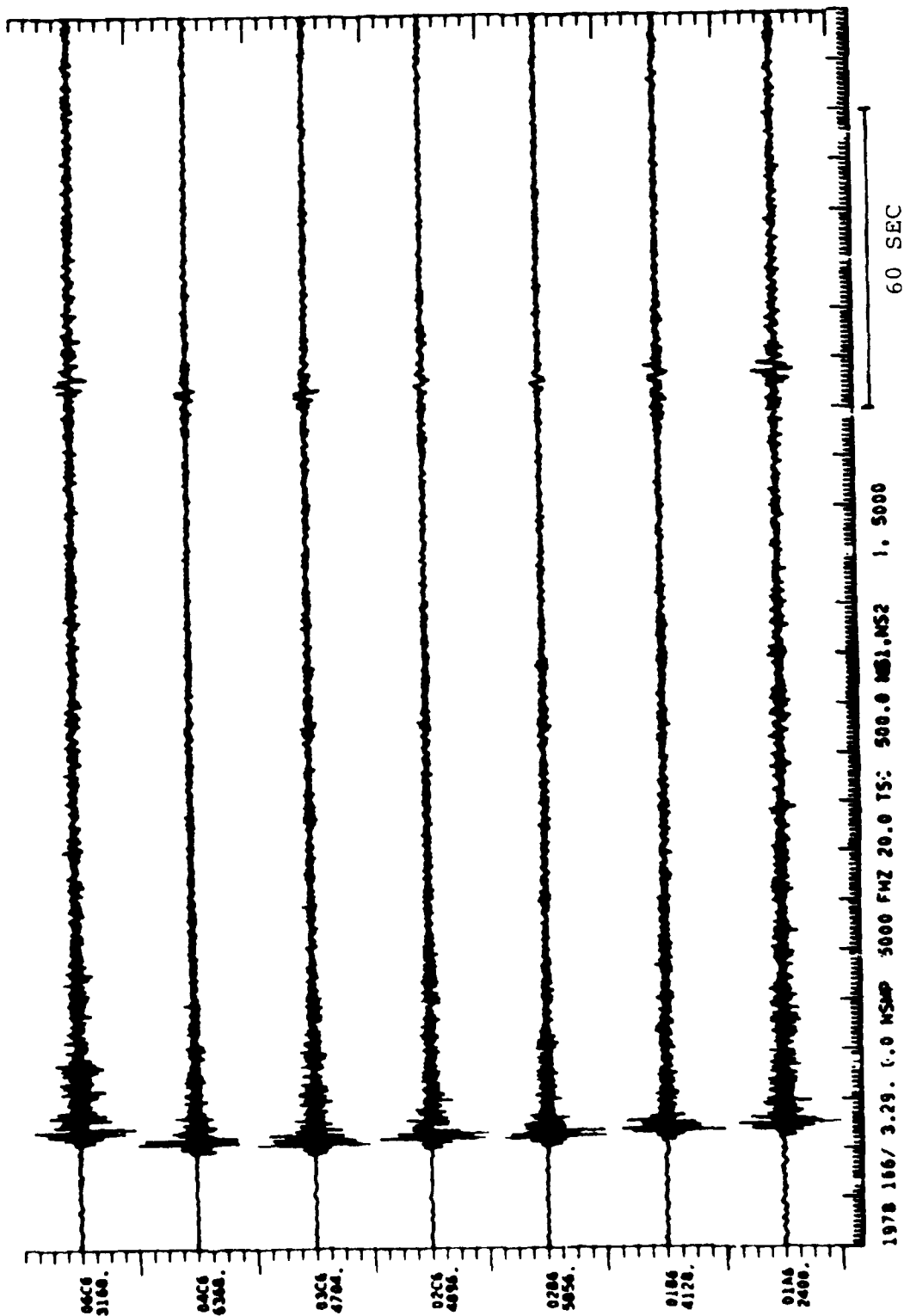| Year	Date	Agency	O.T. (U.T.)	Lat.	Long.	Dep. (km)	mb	Ref. (mb)
1971	Oct25	ISC	0:9:30.5	29.981N	137.195E	514	5.2	ISC
1971	Oct30	ISC	14:16:23.4	32.091N	137.804E	391	5.5	ISC
1972	Oct29	ISC	7:20:39.9	33.067N	137.950E	345	5.3	ISC
1976	Jun25	ISC	7:47:48.4	29.898N	138.745E	455	5.4	ISC
1977	Dec29	ISC	19:45:28.5	28.514N	138.511E	541	5.1	ISC
1978	Jun15	ISC	3:19:9.0	43.408N	135.448E	365	5.2	ISC
1978	Jul10	ISC	6:2:20.6	48.775N	150.123E	341	5.1	ISC
1980	Jan17	ISC	9:21:55.2	28.299N	138.911E	523	5.2	ISC
1980	Dec22	ISC	20:31:44.0	48.180N	146.240E	465	5.3	ISC
1982	Jun23	GS	1:51:54.8	29.062N	138.769E	476	5.3	PDE

Figure 4. Deep focus event recorded at center seismometers, NORSAR array. Numbers beside times give relative amplitudes.

Table 2. Semipalatinsk events recorded at NORSAR.

Year	Date	Agency	O.T. (UTC)	Lat.	Long.	Dep. (km)	m_b	Ref. (m_b)	Comment
1971	Jun6	ISC	4:2:57.3	49.977N	77.740E	0	5.5	ISC	DegelenNW
1971	Jun19	ISC	4:3:57.7	49.966N	77.724E	0	5.4	ISC	DegelenNW
1971	Jun30	ISC	3:57:2.1	49.916N	79.009E	33	5.2	ISC	Shagan
1972	Mar10	ISC	4:56:57.8	49.793N	78.192E	0	5.4	ISC	DegelenSE
1972	Jun7	ISC	1:27:57.4	49.800N	78.156E	0	5.4	ISC	DegelenSE
1972	Aug26	ISC	3:46:56.9	49.943N	77.807E	0	5.3	ISC	DegelenNW
1973	Jul10	ISC	1:26:58.0	49.817N	78.091E	0	5.2	ISC	DegelenSE
1974	May16	ISC	3:2:57.6	49.738N	78.122E	0	5.2	ISC	DegelenSE
1975	Jun8	ISC	3:26:57.6	49.752N	78.080E	0	5.5	ISC	DegelenSE
1975	Jun30	ISC	3:26:57.3	49.980N	78.921E	0	5.0	ISC	Shagan
1976	Mar20	ISC	4:3:39.3	50.020N	77.366E	0	5.1	ISC	Other(?)[1]
1976	Apr21	ISC	5:2:57.3	49.886N	78.830E	0	5.3	ISC	Shagan
1978	Apr22	ISC	3:6:57.7	49.717N	78.176E	0	5.3	ISC	DegelenSE
1980	Jul31	ISC	3:32:58.0	49.815N	78.145E	0	5.3	ISC	DegelenSE

---

[1] Probably a shallow focus (focal depth ∿20 km) earthquake (Pooley et al., 1983).
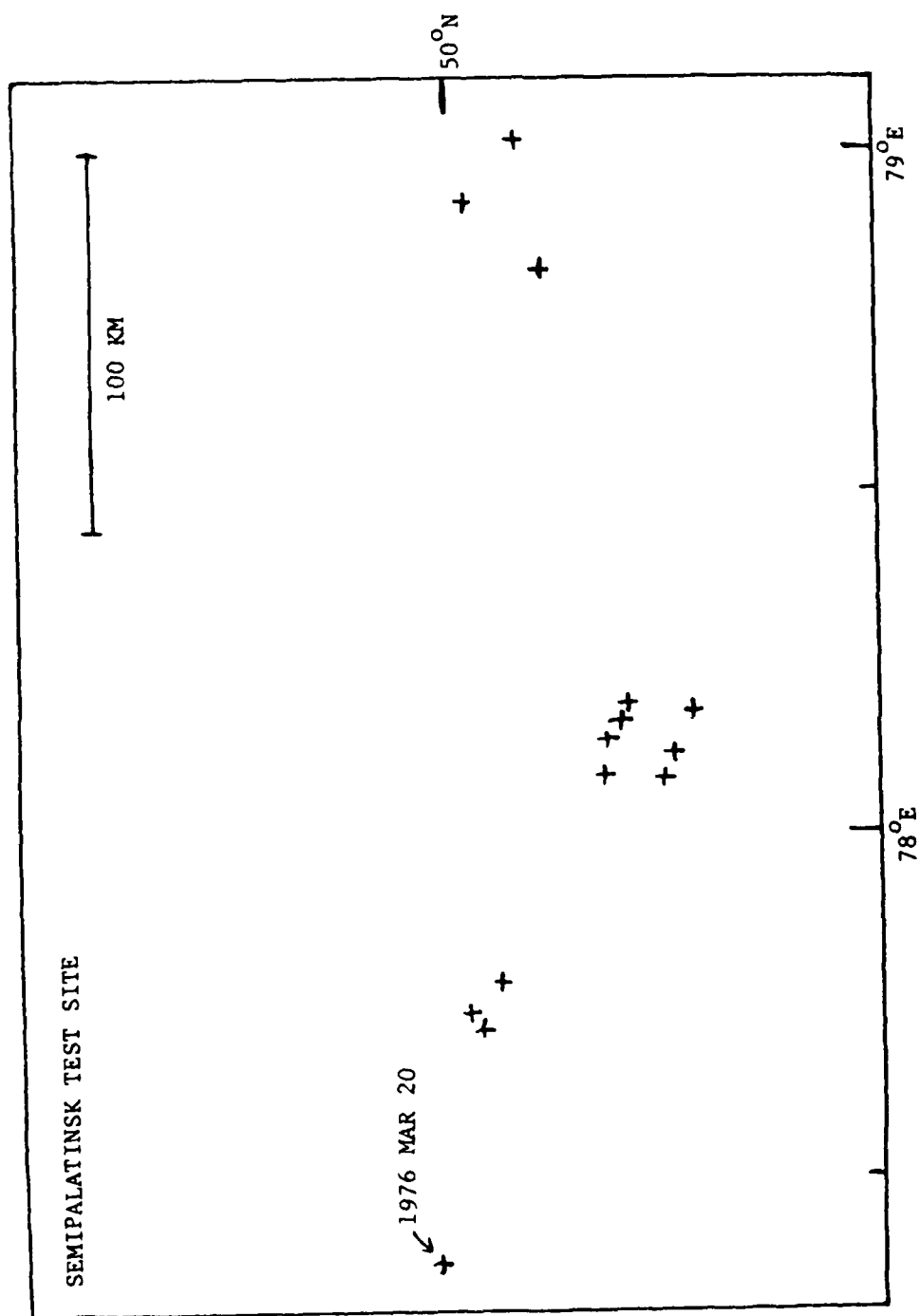
Figure 5. Map of Semipalatinsk Test Site. From right, subareas are Shagan River, Degelen SE, and Degelen NW.

24

SEMIPALATINSK 1978 APR 22

60 SEC

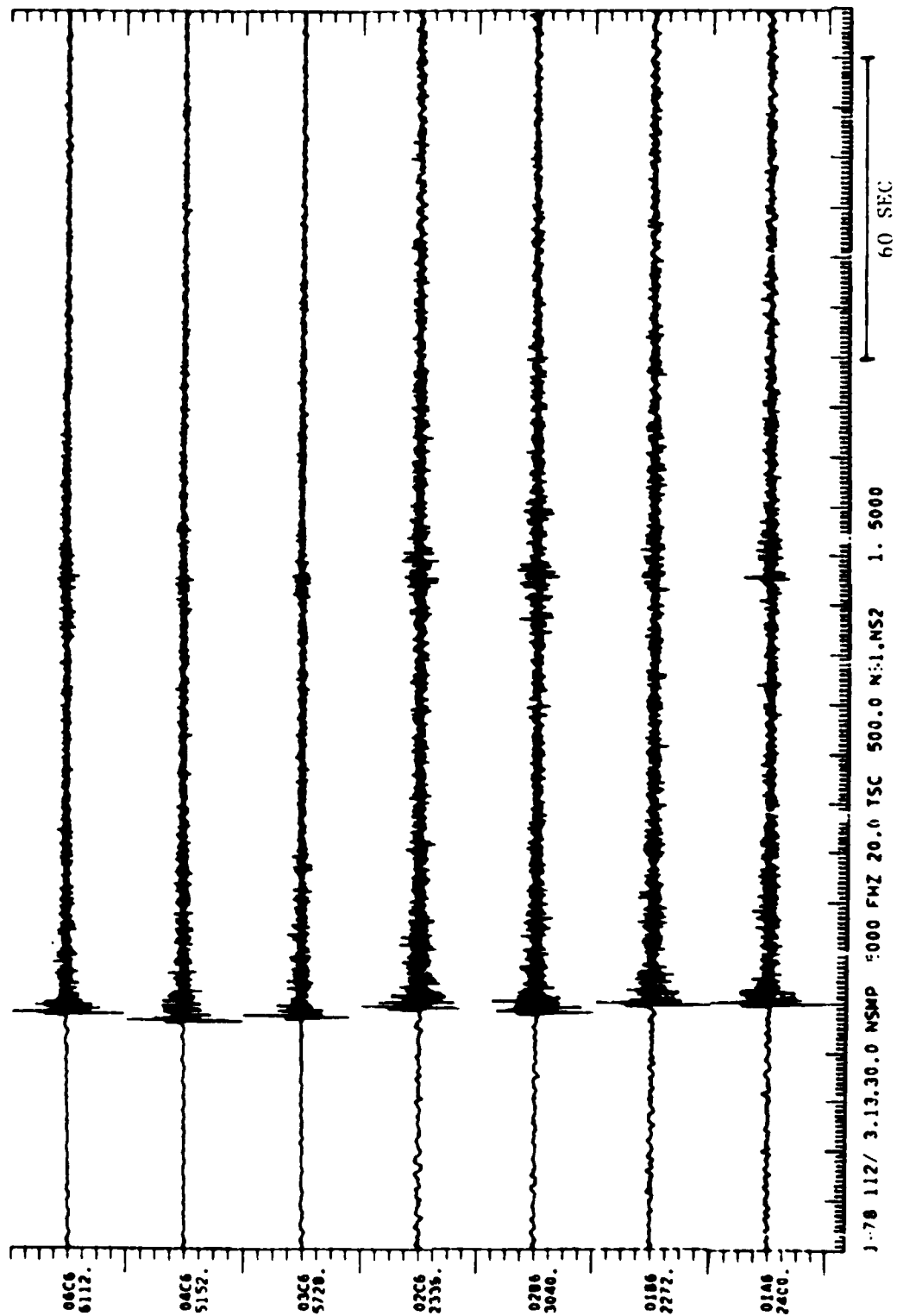J-78 112/ 3.13.30.0 NSMP 5000 FWZ 20.0 TSC 500.0 N:1,NS2 1.5000

Figure 6. Presumed Semipalatinsk explosion recorded at the center seismometer, NORSAR.

TABLE 3. Nevada Test Site Events Recorded at NORSAR.

Year	Date	OT (UTC)	Latitude	Longitude	Depth (km)	m_b	Ref. (m_b)	Comments
1973	Jun 6	13:00:0.1	37.245°N	116.346°W	0	6.1	PDE	"ALMENDRO", PAHUTE
1975	May 14	14:00:0.4	37.221°N	116.474°W	0	6.0	PDE	"TYBO", PAHUTE
1975	Jun 19	13:00:0.1	37.350°N	116.320°W	0	6.1	PDE	"MAST", PAHUTE
1975	Oct 28	14:30:0	N.A.	N.A.	N.A.	N.A.	---	"KASSERI", PAHUTE
1976	Mar 14	12:30:0.2	37.306°N	116.471°W	0	6.3	PDE	"COLBY", PAHUTE
1976	Mar 17	14:15:0.1	37.256°N	116.312°W	0	6.1	PDE	"POOL", PAHUTE
1976	Mar 17	14:45:0.1	37.107°N	116.052°W	0	5.8	PDE	"STRAIT", YUCCA
1978	Sep 27	17:20:0.0	37.074°N	116.020°W	0	5.7	PDE	"RUMMY", YUCCA
1982	Aug 5	14:00:0.0	37.084°N	116.007°W	0	5.7	PDE	"ATRISCO", YUCCA

Figure 7 shows one of the explosions. Table 4 shows events recorded at NORESS.

Analysis Methods

The two arrays, NORSAR and NORESS, are shown in Figures 8 and 9. Each subarray in NORSAR consists of one three-component LP station (not used in this study) and six SP components; one SP component is near the center of the subarray and the other five are arrayed more or less equally spaced on a circle of radius ~4 km around the center. Ringdal (1981) gives the NORSAR instrument response; the NORESS instrument response is similar to the NORSAR SP but extends to higher frequencies. Mykkeltveit et al. (1983) and Ingate et al. (1985) discuss the design concepts behind the NORESS array.

The NORSAR data used were the outputs of the 12 seismometers of subarrays 02B and 03C, unless the majority of the seismometers on one of the subarrays clipped on first P, in which case that subarray was not used. These outputs were treated as independent seismograms and were analysed using the methods of Dainty et al. (1984) to fit (15) and (17). Briefly, a 128 point (6.35 sec) window was moved 64 points (3.2 sec) at a time down the seismogram, starting at the beginning of data. The Fourier transform of the ground motion was taken and the amplitude averaged over a one-octave band about a specified center frequency; this value of the amplitude was taken as proportional to the square root of the power spectrum. The $\log_{10}$ of the amplitude was plotted as a function of time to the window center to check the data--Figure 10 shows an example. The Fourier amplitude of the first P pulse was found by
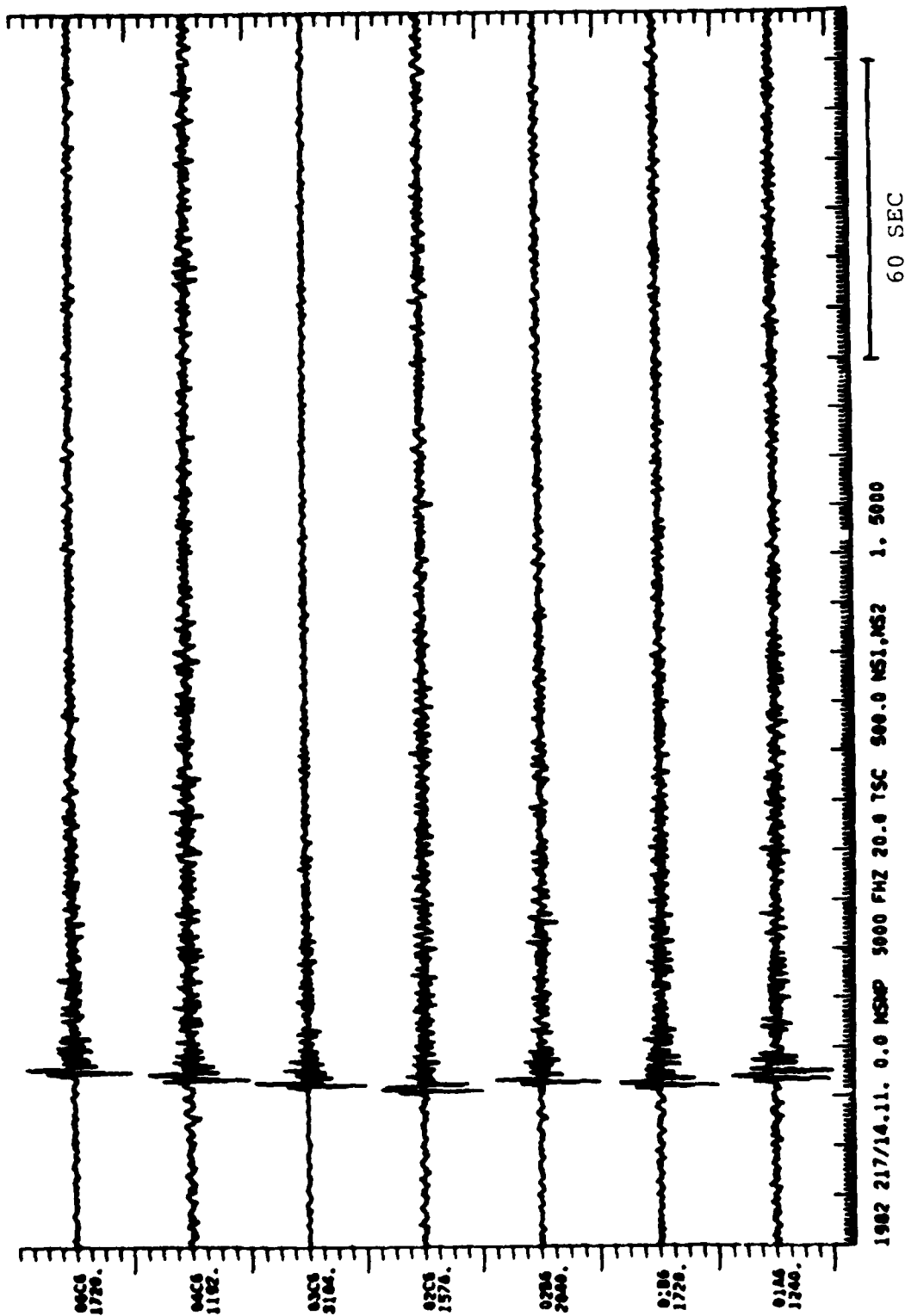
Figure 7. Nevada Test Site explosion "ATRISCO" recorded at center seismometer, NORSAR.

TABLE 4. Events Recorded at NORESS.

Year	Date	OT (UTC)	Latitude	Longitude	Depth (km)	m_b	Agency	Comments
1984	Nov 17	18:27:13.1	28.286°N	139.849°E	465	5.3	PDE	Bonin
1985	Jan 7	16:13:5.2	27.216°N	92.013°E	11	5.6	PDE	Himalaya
1985	Feb 10	03:27:7.6	49.877°N	78.816°E	0	5.9	EDR	Semipalatinsk
1985	Feb 20	17:41:27.3	35.935°N	70.953°E	94	5.1	EDR	Hindu Kush
1985	Mar 9	14:08:4.1	66.215°N	150.063°W	12	5.9	PDE	Alaska
1985	Apr 10	16:26:18.6	29.979°N	138.790°E	398	5.8	PDE	Honshu
1985	Apr 18	5:52:52.7	25.898°N	102.870°E	5	5.7	PDE	Yunnan
1985	Apr 25	00:57:6.5	49.907°N	78.932°E	0	5.9	PDE	Semipalatinsk
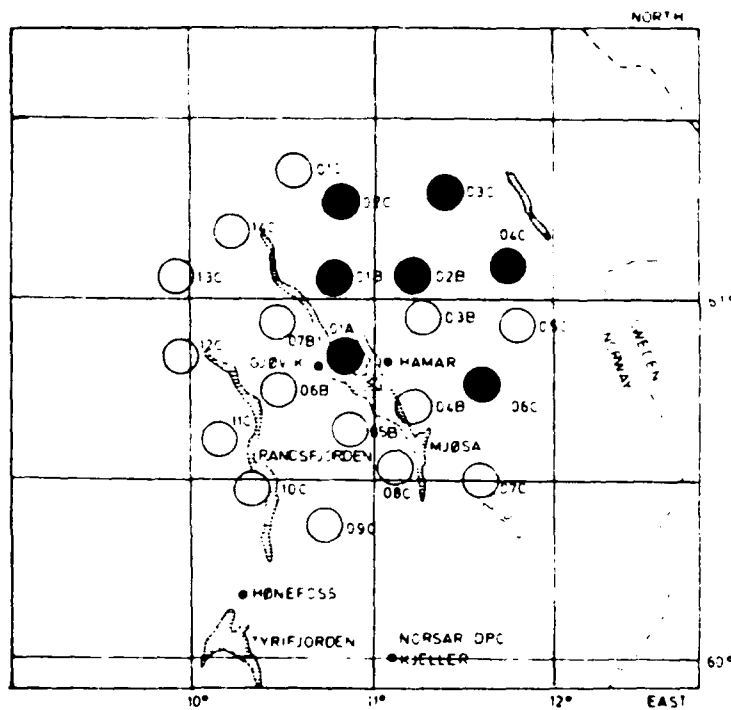
Figure 8. Map of NORSAR subarrays. All subarrays were operational from 1971 to 1976; since 1976 subarrays shown in solid symbols have been operational. The NORESS array is within subarray 06C.

MAP OF ARRAY ELEMENT LOCATIONS
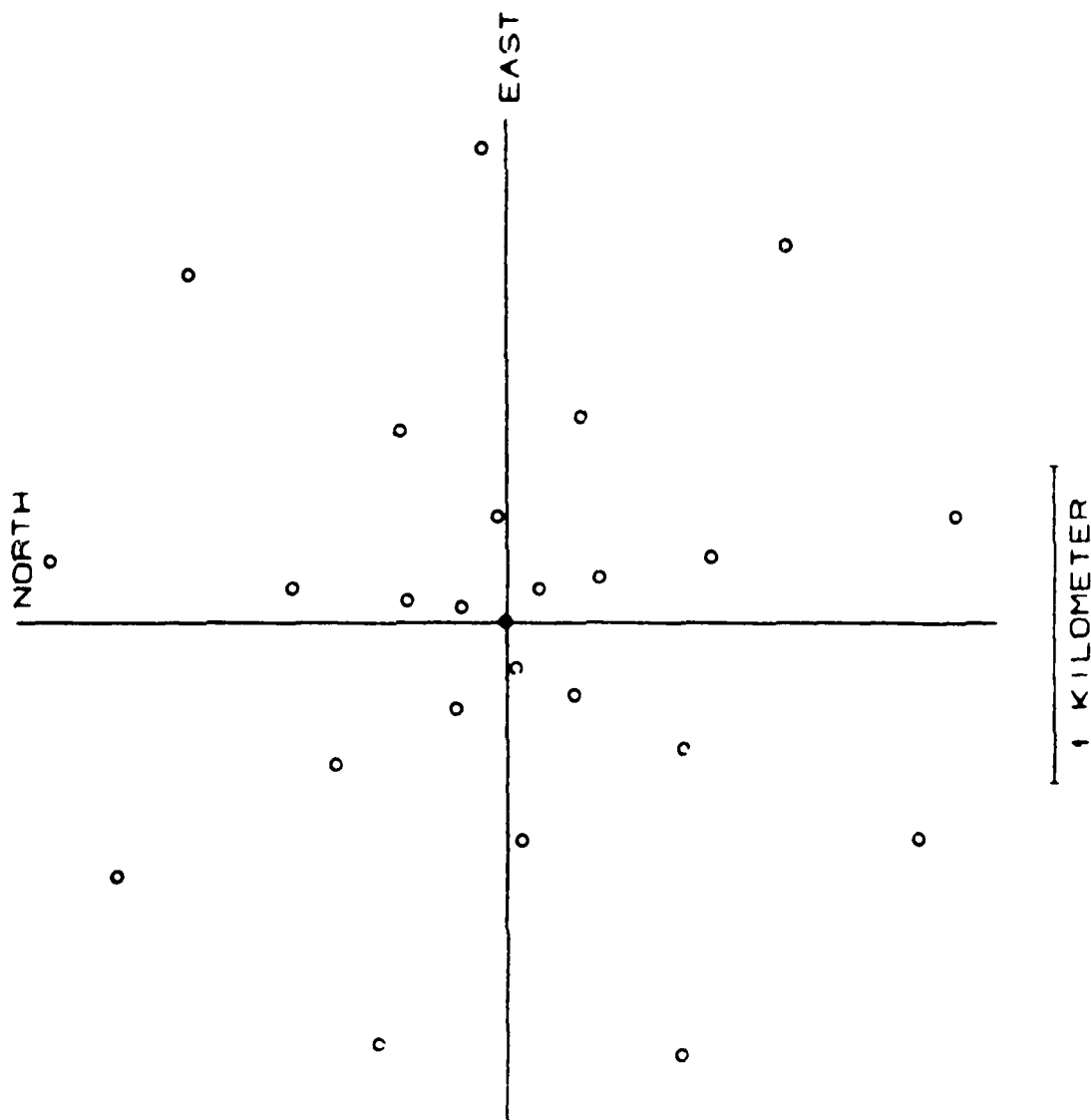
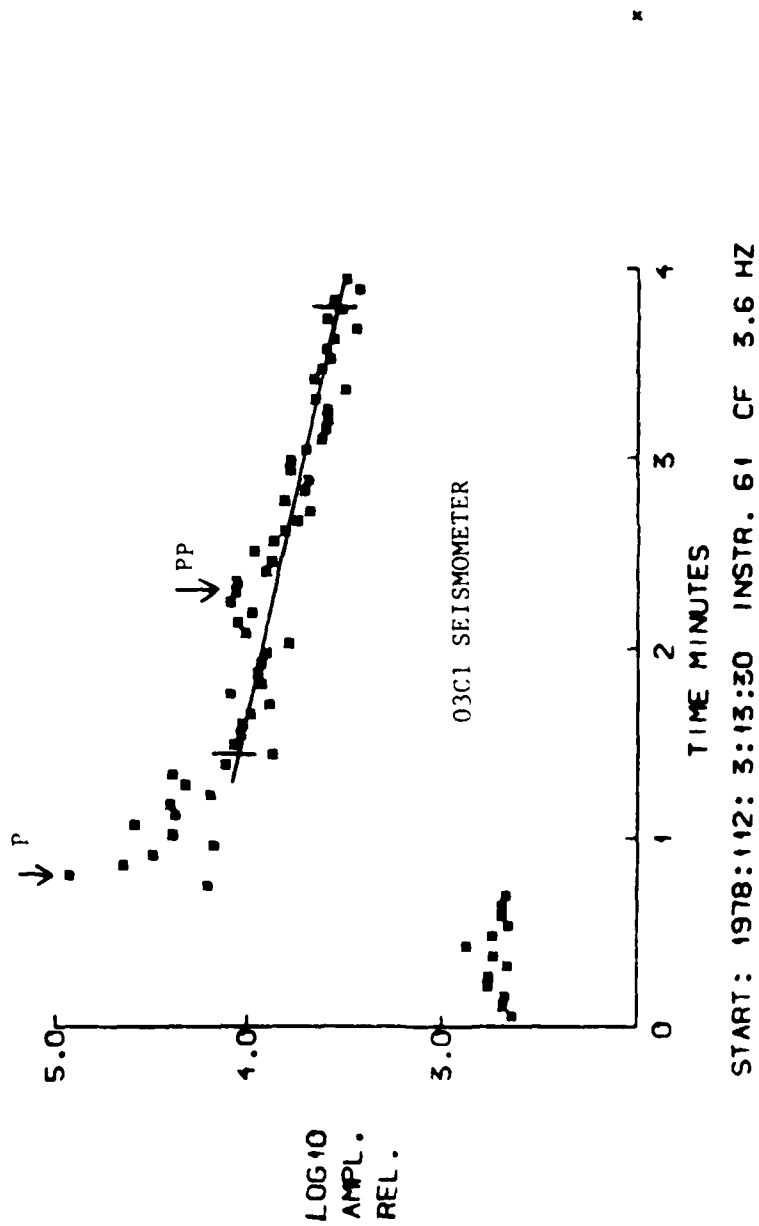Figure 9. Map of NORESS array seismometer sites. See Figure 8 for location of NORESS.

START: 1978:112: 3:13:30 INSTR. 61 CF 3.6 HZ

Figure 10. Fourier amplitude as a function of time at NORSAR for presumed Semipalatinsk explosion shown in Figure 6, at 3.6 Hz.

finding the two points nearest the time of first P onset, and taking the largest of them. Relations (15) and (17) were fitted to data like that shown in Figure 10 for a time interval that started at least 20 sec after first P, was at least 60 sec long, and within which the signal was at least 10 dB above the noise. The goodness of fit (as measured by the mean square error), $\overline{Q}$, G_a, G, and G' were tabulated for each seismogram and center frequency. The average of $1/\overline{Q}$, $\log_{10} G$, and $\log_{10} G'$ were taken in various combinations for interpretation purposes; this assumes that $1/\overline{Q}$, which is proportional to the rate of coda decay with time, is normally distributed and that G and G', which are proportional to the ratio of coda power to first P energy, are log normally distributed. These are conventional assumptions.

The NORESS data (Table 4) was analysed both by the method described above and by frequency-wavenumber analysis. Analysis of the coda power as a function of time was carried out as described in the preceding paragraph, except that a 128-point window is 3.175 sec long, a 64-point shift is 1.6 sec, and data lengths of 30 sec and greater were accepted for fitting.

The frequency-wavenumber (f-k) analysis used began with a conventional single-frequency two-dimensional wavenumber spectrum. A discussion of the use of this analysis is given in Aki and Richards (1980), section 11.4. Mykkeltveit and Ringdal (1981) and Mykkeltveit and Bungum (1984) show examples. Figure 11 shows an analysis window in the coda of a large Semipalatinsk presumed explosion and Figure 12 the resulting single-frequency f-k spectrum. The contour levels indicate the power at a given wavenumber East (kx) and North (ky). Linear
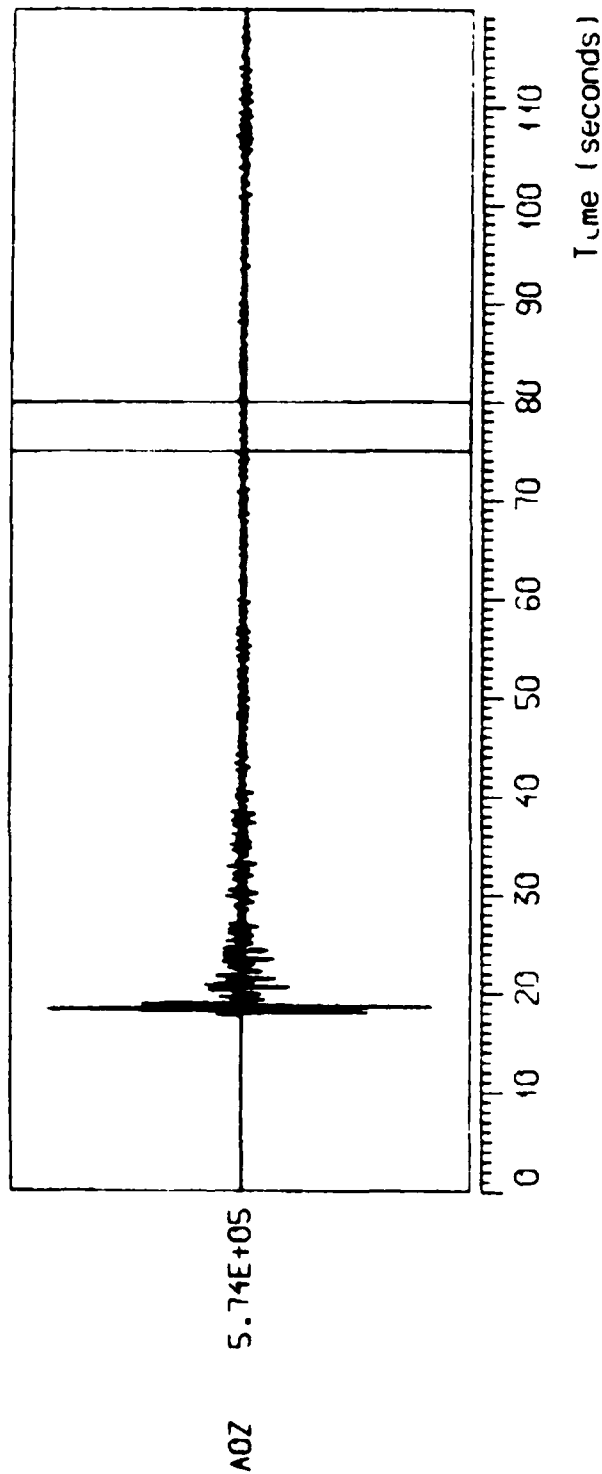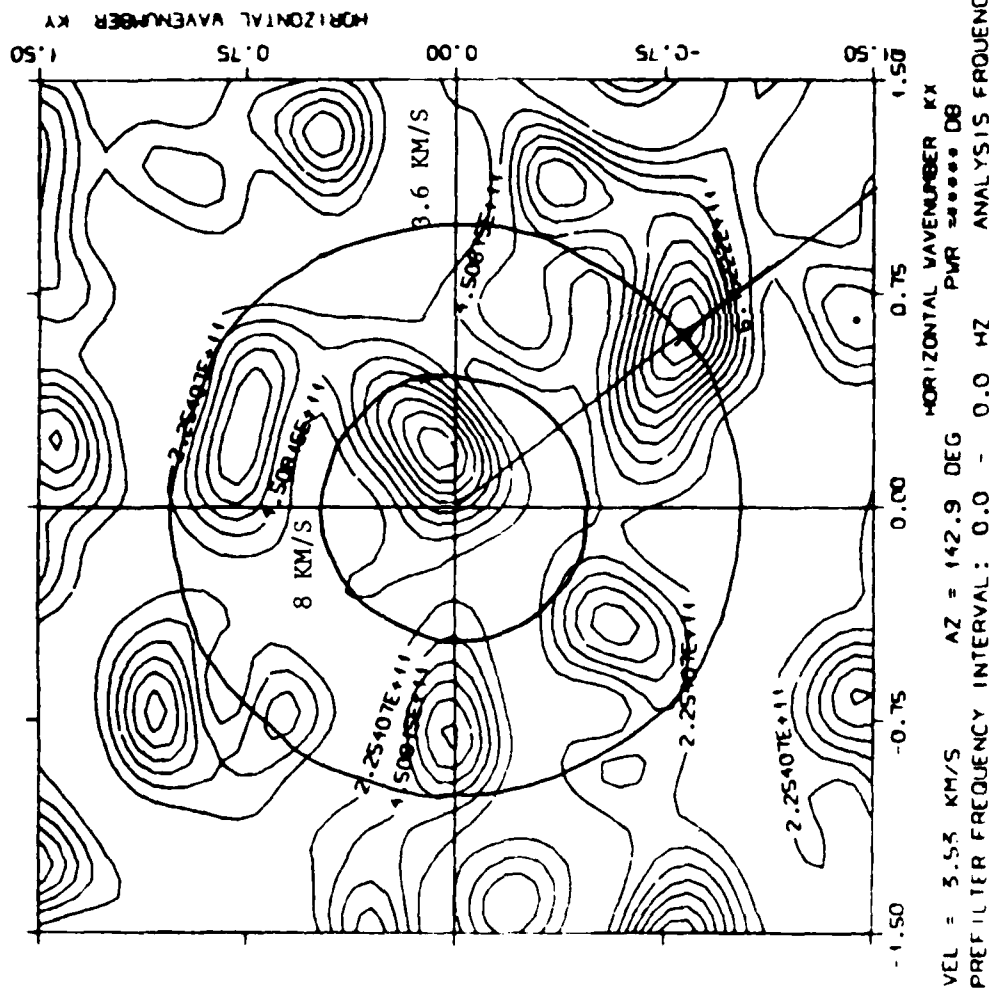
Figure 11. Presumed Semipalatinsk explosion as recorded at the center seismometer, NORESS, with an analysis window shown. The same window is applied to the seismograms of all 25 verticals.

Figure 12. Single frequency f-k analysis at 3.6 Hz, for event and window of Figure 11. Contours are power, in (bits)^2. See text for discussion.

wavenumbers are used (i.e., wavenumber = 1/wavelength) throughout and are given in cycles/km; North and East are positive. Figure 12 shows peaks in the contour plot, indicating a wave coming with particular kx, ky. The azimuth θ of such a wave is measured clockwise from North and is given by

$$\tan\theta = ky/kx \tag{22}$$

The total horizontal wavenumber k is given by

$$k^2 = kx^2 + ky^2 \tag{23}$$

and the phase, or apparent velocity, is

$$V_{app} = f/k \tag{24}$$

The power spectrum shown in Figure 12 is a section at constant frequency of a three-dimensional Fourier transform (one time dimension and two space dimensions). In a practical situation where the wavefield is sampled both in space and time over restricted intervals in space and time, these constraints affect the precision with which the spectrum may be determined. The principal concern in this study is the spatial limitations, which are set by the position of the array seismometers (Figure 9). The smallest spacing Δr_{min} between seismometers determines the shortest wavelength λ_{min} that may be examined. Theoretically, λ_{min} must be twice Δr_{min}, and in practice should be four or five times Δr_{min}. If the slowest physically realistic phase velocity is assumed to be 3 km/sec, and the highest frequency of interest is 7.2 Hz, this gives a λ_{min} of 0.4 km, while Δr_{min} is 0.15 km. This appears to be

satisfactory, especially since most analyses were conducted at lower frequencies and thus longer wavelengths.

The other effect of the spatial arrangement of seismometers is the total linear span, or aperture, which is about 3 km. The effect of this is to limit the resolution that may be achieved in determining the spectrum, and to produce sidelobes. Figure 13 shows the array response, i.e., the spectrum, for a pure plane wave (of any frequency) vertically incident (infinite phase velocity). Sidelobes are seen at about k = 2 --this is not a problem for most of the analyses that follow. Of more concern is the width of the central peak, about 0.5 cycle/km. This means that peaks have to be about 0.5 cycle/km apart to be resolved, and since by (24) for a given apparent velocity the frequency decreases with wavenumber, 1 Hz is an effective lower limit for analysis, and even at this frequency there are problems with resolution.

The type of plot shown in Figure 12 illustrates two other calculations that may be made. From (23) and (24) a circle centered on the origin in Figure 12 is a line of constant wavenumber and also constant apparent velocity, and from (22) a straight line passing outwards from the origin is a line of constant azimuth. Integrating the spectrum around such circles and lines allows a determination of the power as a function of k (or apparent velocity) and azimuth. Such integrations may be found explicitly in terms of sums of zero-order Bessel functions (apparent velocity) and sinc functions (azimuth) (D. B. Harris, personal communication). Figures 14 and 15 show examples for the same Semipalatinsk event and window as shown in Figure 12. A problem will be noted, however. It appears that, in practical
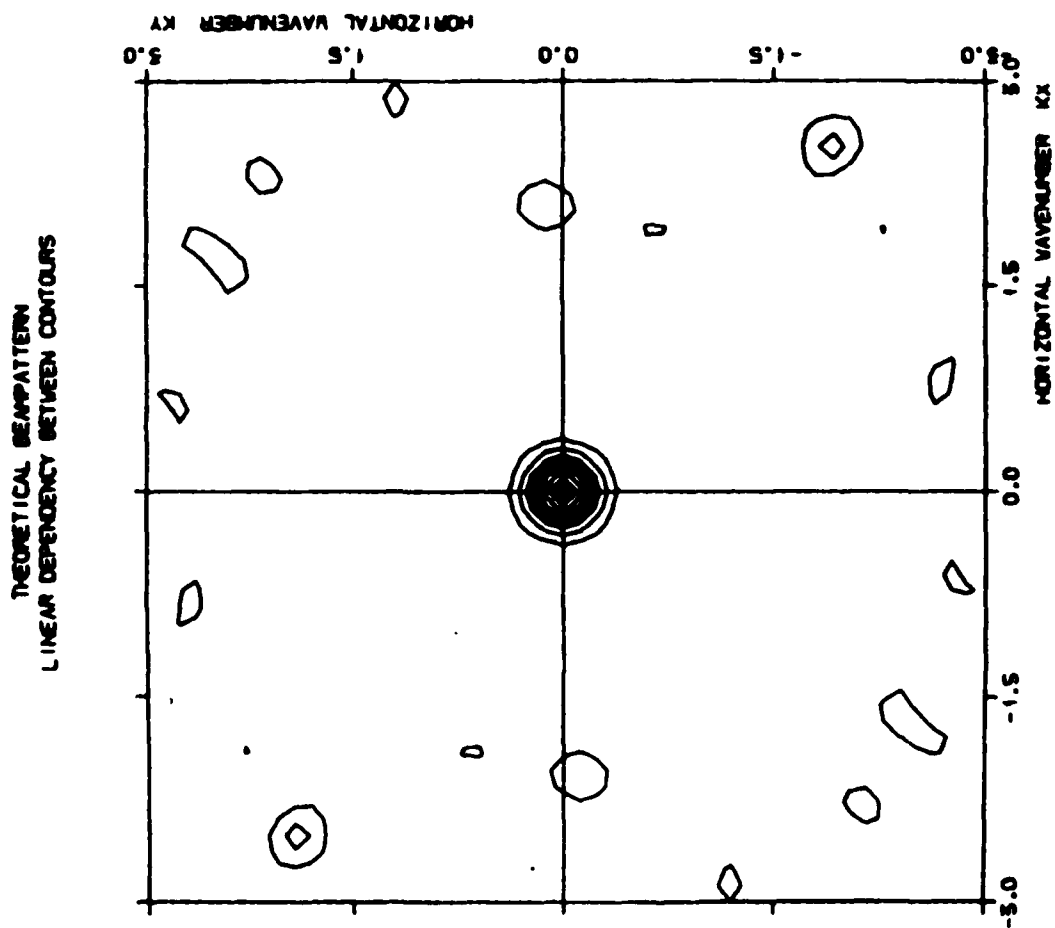
Figure 13. Theoretical beam pattern of the NORESS array. Wavenumbers are linear wavenumbers in km^{-1}, wavenumber = 1/wavelength.
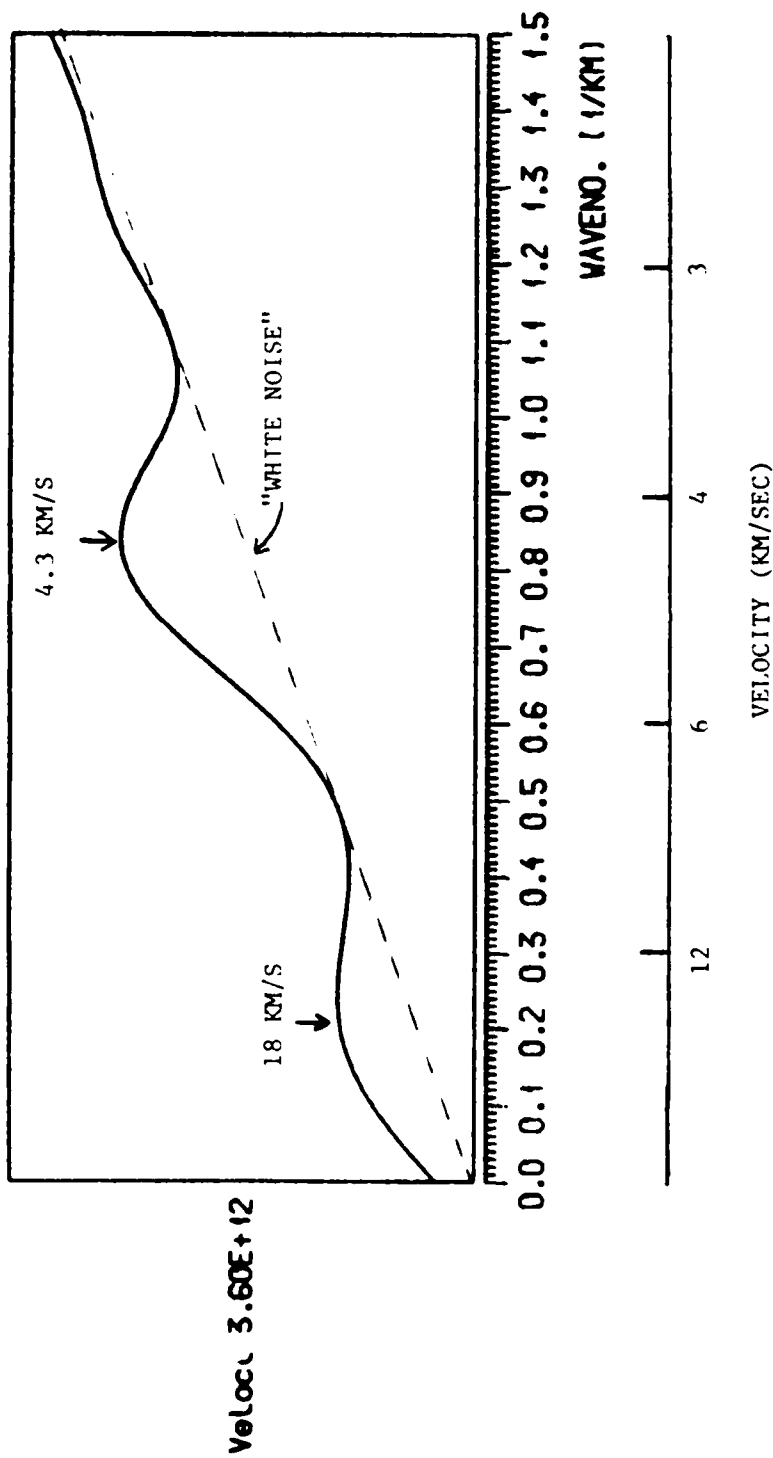
Figure 14. Wavenumber (apparent velocity) spectrum of event and window of Figure 11.
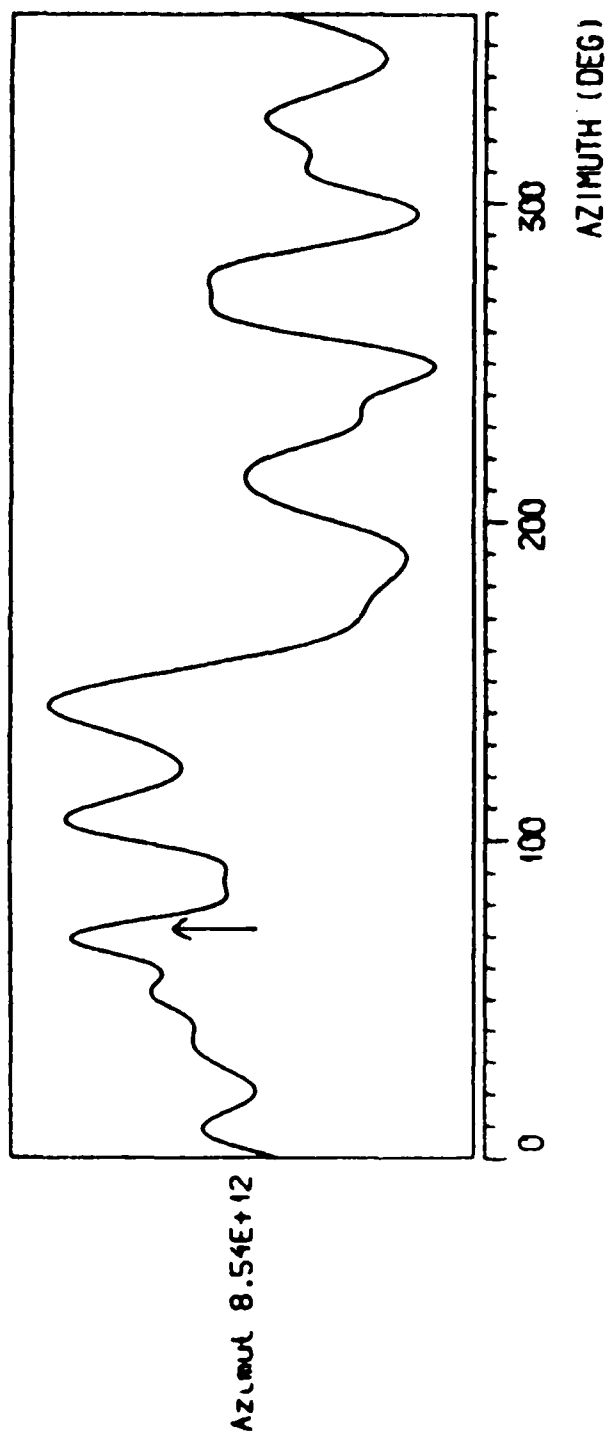See text for discussion.

SEMIPALATINSK 1985 FEB 10

Figure 15. Azimuth spectrum of event and window of Figure 11. Arrow indicates source azimuth. See text for discussion.

terms, there is always a "white noise" component on the f-k spectrum, i.e., a constant background that does not depend on kx, ky. Since the circumference of the circle shown in Figure 12 increases with increasing k (or decreasing apparent velocity, by (24)), the power due to the white noise background will increase linearly with increasing k; such an effect seems to be present in Figure 14. Also, the presence of such a background will produce a "floor" under the azimuth integration, as seen in Figure 15. Nonetheless, Figure 14 especially seems to indicate the power of this method to separate high and low apparent velocity parts of the coda.

The f-k, power-wavenumber, and power-azimuth calculations were carried out using an analysis package developed by David Harris of Livermore National Laboratory and Tormod Kvaerna of NORSAR, at NORSAR. An addition to the analysis was the use of decay-corrected averages in the coda, since at a given frequency the theory presented predicts that in the time frame considered, the coda is stationary in the statistical sense in time and space. To obtain the averages, a five-second window was moved down the coda (not overlapping) and the power at each value of kx, ky (f-k spectra), k (wavenumber or apparent velocity spectra), or azimuth (azimuth spectra) was averaged after being normalised to the time of the first window by multiplying by

$$N_i = \exp[2\pi f(t_i - t_1)/\overline{Q}] \qquad (25)$$

where t_i is the time to the center of window i, t_1 is the time to the center of the first window considered, and $\overline{Q}$ is the value found by fitting (15). All f-k spectra, wavenumbers spectra, and azimuth spectra

were determined using the full array of vertical seismometers shown in

Figure 9.

RESULTS

Coda Power as a Function of Time

All the events (Tables 1, 2, 3, and 4; Figure 3) were fit to
equations (15) and (17), as described in the previous section. In
making this fit, it was usually found that while the goodness of fit was
about the same for both cases, fits of equation (17) often gave
physically unrealistic negative values for Q, whereas fits of equation
(15) almost always gave positive values. In conjunction with the NORESS
evidence to be presented, this would indicate that horizontally confined
spreading (i.e., two-dimensional spreading) is the dominant mode in the
coda, and accordingly only values of $\log_{10}G$ and $\overline{Q}$ from fits of (16)
will be presented here. Fits were attempted at center frequencies of
0.9, 1.8, and 3.6 Hz for NORSAR data, and at 0.9, 1.8, 3.6, and 7.2 Hz
for NORESS data. Because of signal-to-noise problems, it was not always
possible to get meaningful results.

The results for NORSAR data are presented in Table 5 in the form of
averages. The question of whether it was appropriate to average results
was carefully considered by making comparisons between different instru-
ments and different events. In all cases where averages have been
taken, the values determined for individual events or seismometers did
not differ from each other by a statistically significant amount. It
will be noted that not all frequencies for all events are fit. This is
because the twin requirements of no clipping on first P, and at least
10 dB signal-to-noise ratio for 60 sec starting 20 sec after first P
onset are quite onerous at NORSAR. Generally, signal-to-noise tends to

TABLE 5. Results of Fits of Coda Power as a Function
of Time to NORSAR Records.

Event Type	Frequency (Hz)	$\overline{Q}$	$G_a(km^{-1})$	$\log_{10}G(km^{-1})$
Deep-focus, Bonin-Japan-Kuriles-Kamchatka	3.6	850+50	0.0067	-3.3+0.1
Presumed Semipalatinsk Explosions	3.6	1200+150	0.0047	-3.3+0.3
Semipalatinsk Crustal Earth-quake, 1976 March 20	3.6	1200+250	0.0047	-1.6+0.3
Nevada Test Site Explosions	0.9	200+15	0.0071	-2.9+0.2
	1.8	400+60	0.0071	-3.4+0.2
	3.6	1250+450	0.0045	-3.1+0.1

increase with increasing frequency, but the frequency spectrum of the event also plays a part--Nevada Test Site (NTS) events are lower frequency than the others. The significance of the results will be discussed in the next section.

Results for NORESS are given in Table 6. Since fewer events are involved, values are quoted for each event, averaged over the central nine seismometers of the array. Since the dynamic range of NORESS is much greater than NORSAR, larger events may be used without clipping, which eases the signal-to-noise ratio problem. The requirement of only 30 sec of coda after 20 sec after first P onset also helps the situation, and fits are often possible for frequencies that could not be used on the NORSAR data.

Power as a Function of Apparent Velocity at NORESS

Results for the f-k analysis are presented for the events in Table 4. Because of the large amount of data reduced, only calculations relevant to the discussion shall be shown. Six events are selected: two Semipalatinsk explosions, two shallow focus earthquakes (Alaska and Yunnan), and two deep focus earthquakes (Bonin and Honshu). Figure 16 shows the seismograms from these events recorded at the center seismometer of the NORESS array and Figure 17 shows the power spectra, taken in a short window around first P. Figures 18 through 23 show the f-k spectra at a frequency that is either at a peak of frequency or at 1 Hz if the frequency peak (Figure 17) is at a lower frequency than 1 Hz. Each figure shows a single f-k spectrum for a window around first P and an average f-k spectrum for the coda. Figures 24 through 29 show the

TABLE 6. Results of Fits of Coda Power as a Function
of Time to NORESS Records.

Event	Frequency (Hz)	$\overline{Q}$	$G_a(km^{-1})$	$\log_{10}G(km^{-1})$
Bonin, 1984 November 17	7.2	2200+600	0.005	-2.8+0.2
Himalaya, 1985 January 7	1.8	350+60	0.0081	-3.4+0.1
	3.6	1150+250	0.0049	-2.8+0.1
Semipalatinsk, 1985 February 10	1.8	400+70	0.0071	-4.4+0.1
	3.6	1100+500	0.005	-3.8+0.2
	7.2	1500+200	0.0075	-3.65+0.15
Hindu Kush, 1985 February 20	1.8	1100+300	0.0026	-2.5+0.1
	3.6	1100+100	0.0051	-3.1+0.05
Alaska, 1985 March 9	0.9	330+30	0.0043	-1.9+0.1
	1.8	660+120	0.0043	-1.9+0.1
	3.6	1250+150	0.0045	-1.9+0.1
Yunnan, 1985 April 18	0.9	160+10	0.0088	-2.6+0.05
	1.8	216+7	0.013	-2.4+0.03
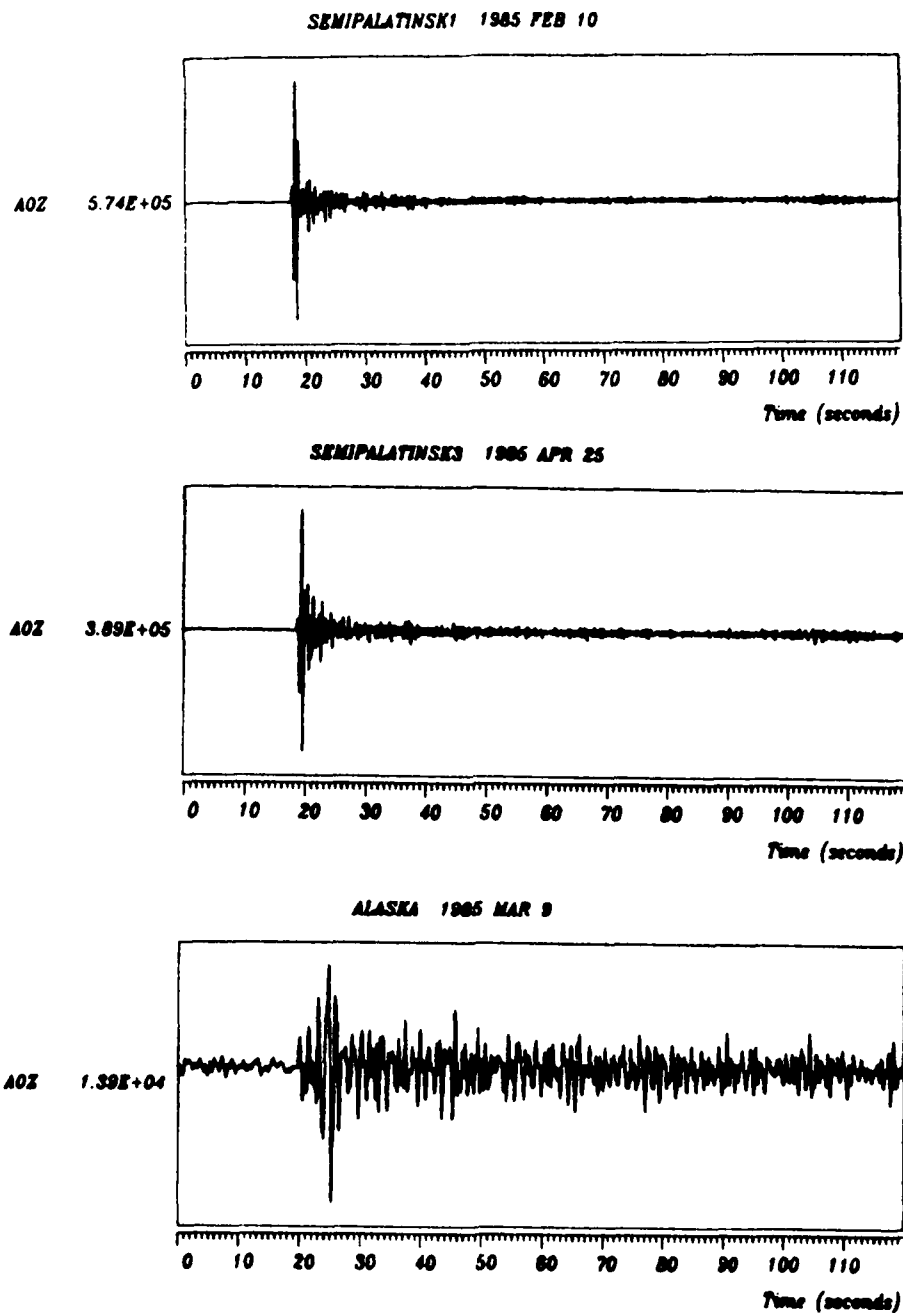
Figure 16a. Events analysed by f-k and wavenumber spectra, as recorded at the center seismometer, NORESS. Time zero is: for Semipalatinsk 1, 3:34:5 (U.T.); for Semipalatinsk 3, 1:4:10; for Alaska, 14:17:0. See Table 4 for further details.
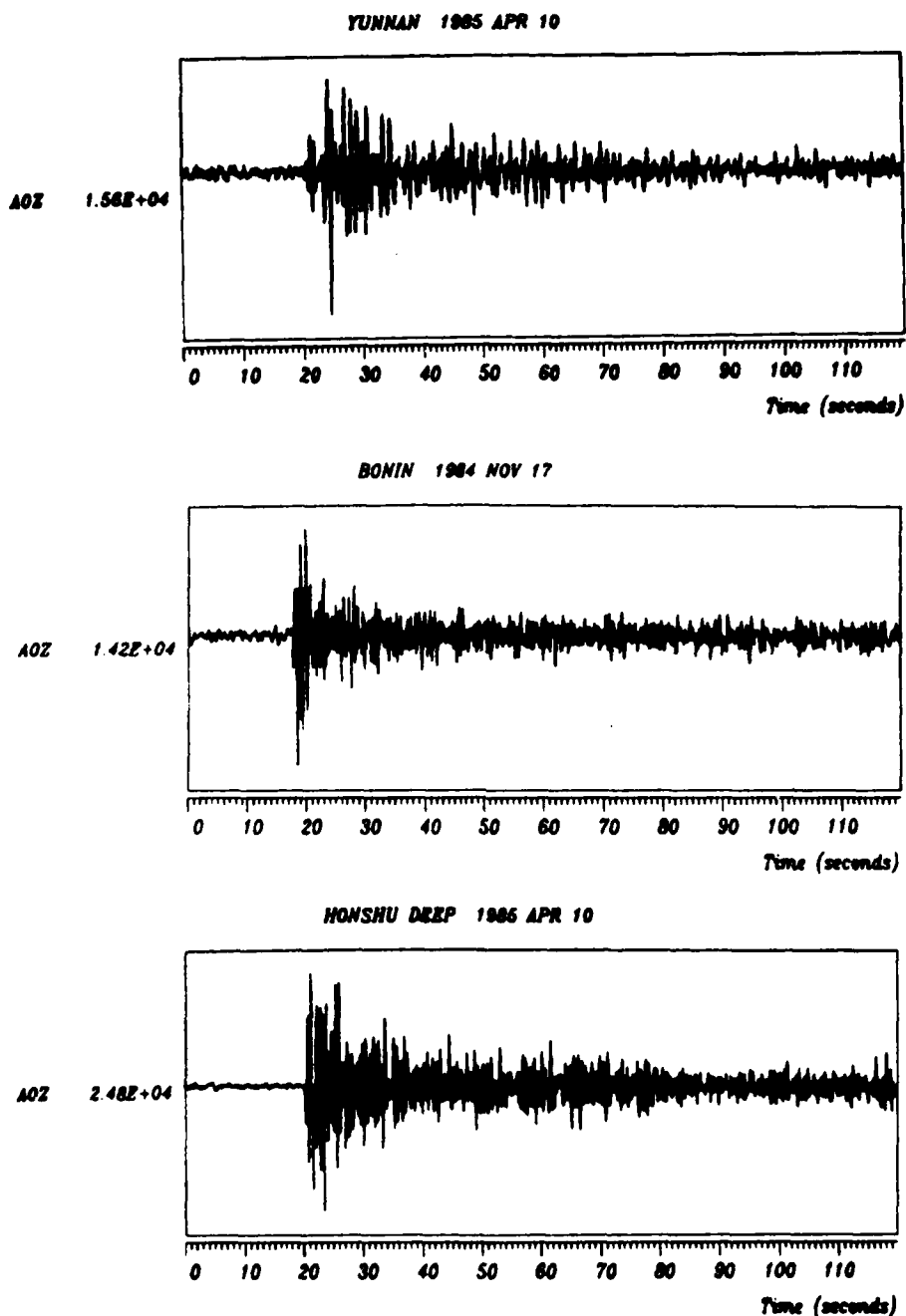
Figure 16b.   Events analysed by f-k and wavenumber spectra, as
recorded at the center seismometer, NORESS. Time zero
is: for Yunnan, 6:3:35 (U.T.); for Bonin, 18:38:25;
for Honshu, 16:37:25. See Table 4 for further details.
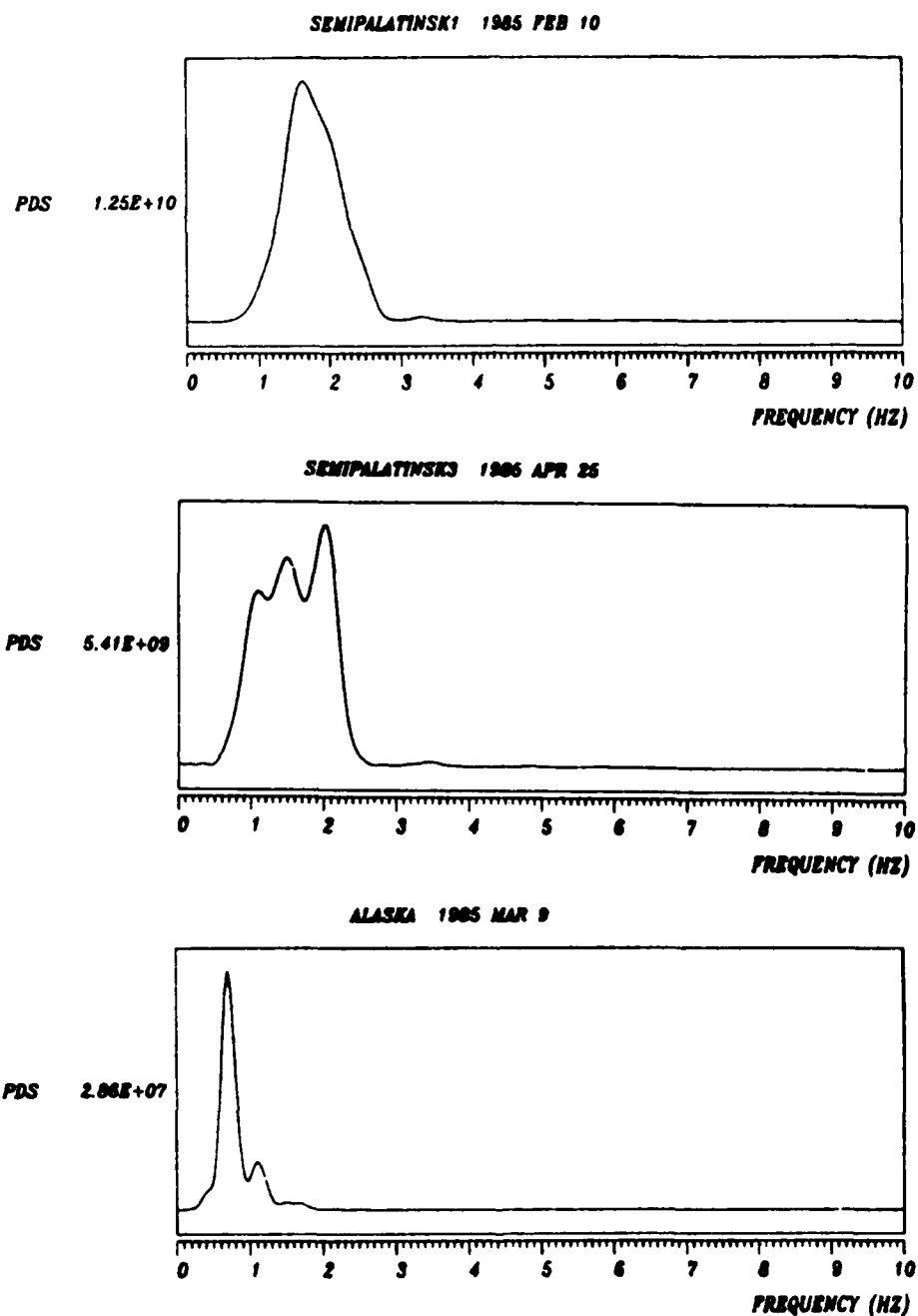
Figure 17a. Power density spectra, events of Figure 16a. Window
~5 sec around first P of center seismometer, NORESS.
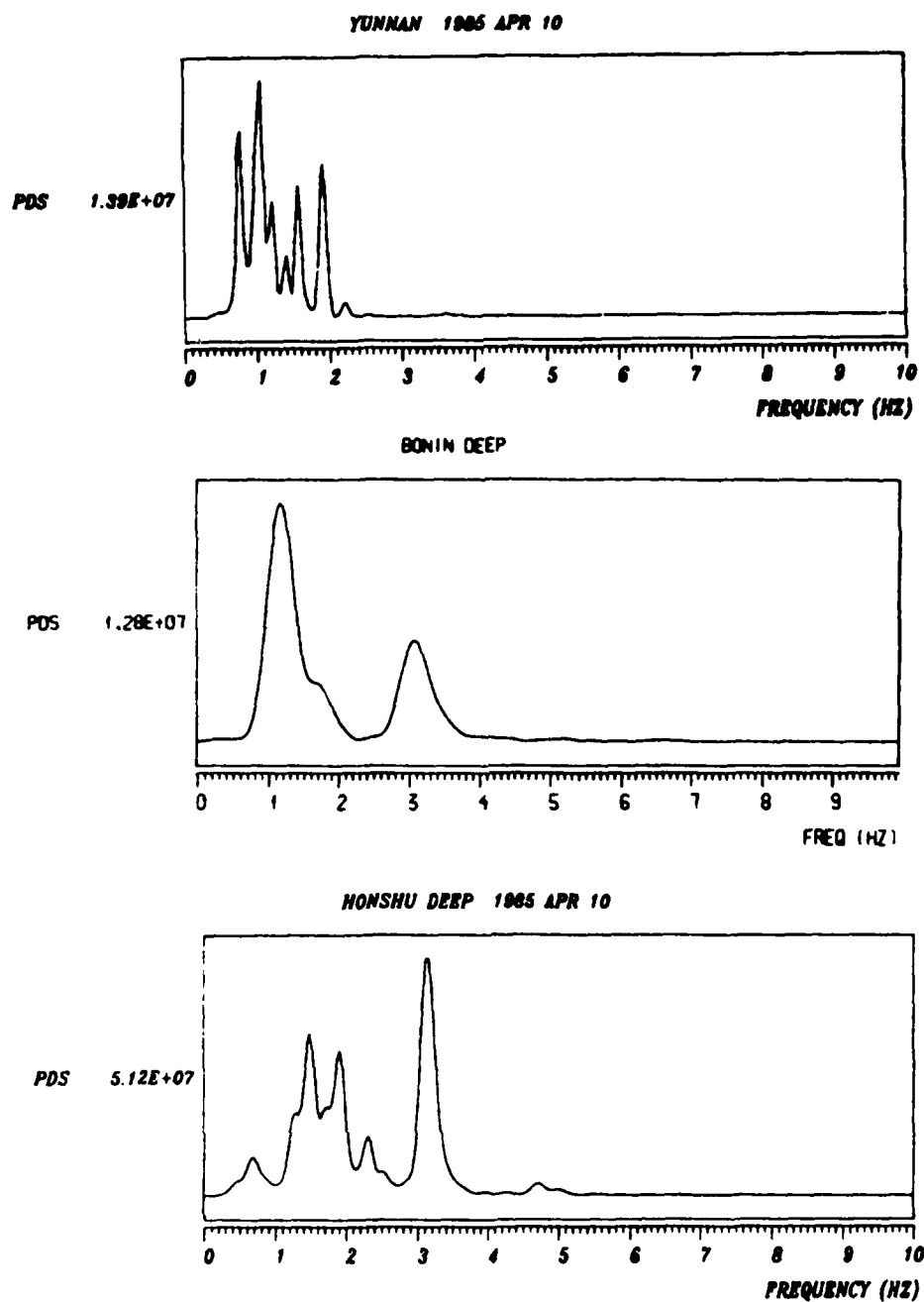
Figure 17b.   Power density spectra, events of Figure 16b.   Window
∿5 sec around first P of center seismometer, NORESS.
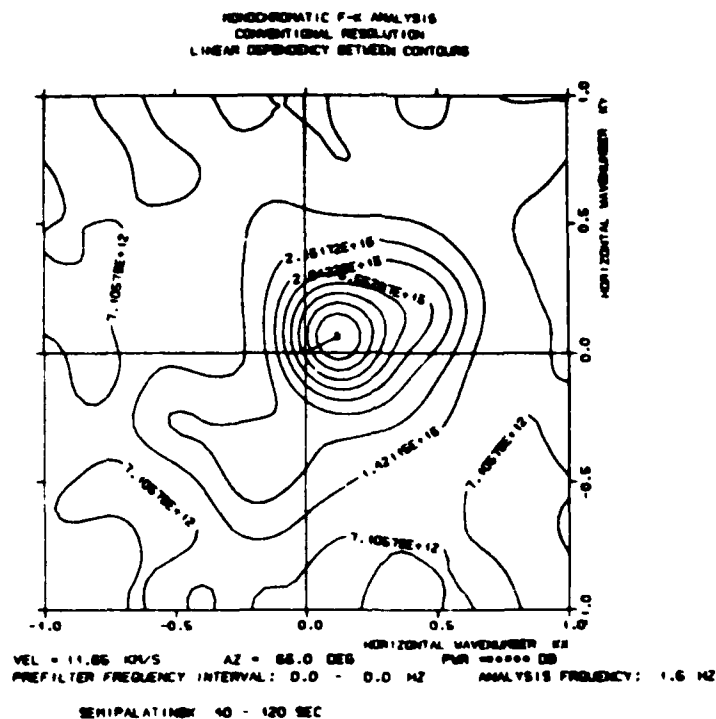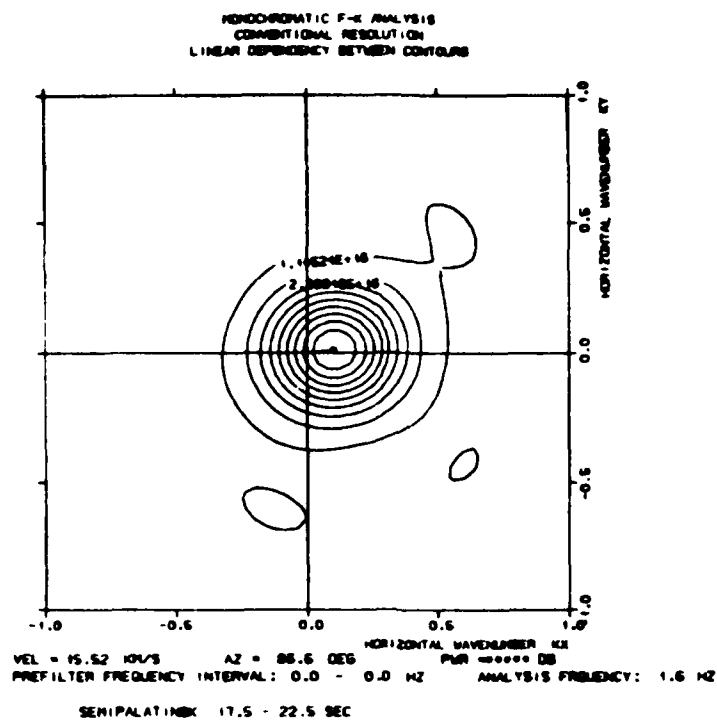
Figure 18. Single frequency f-k spectra, Semipalatinsk, February 10. Time interval (17.5-22.5 sec, top; 40-120 sec, bottom) and frequency (1.6 Hz) written on figure. See Figure 16a for times. See text for discussion.
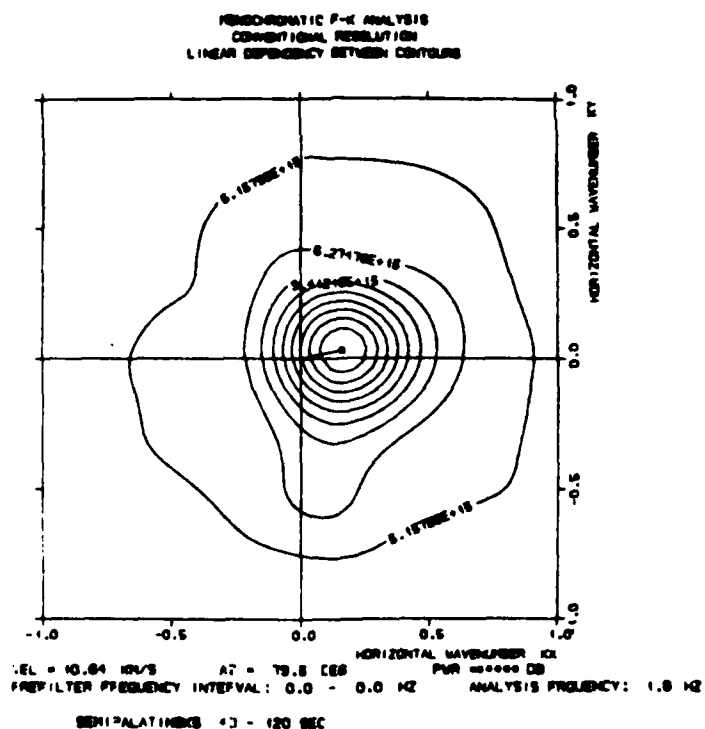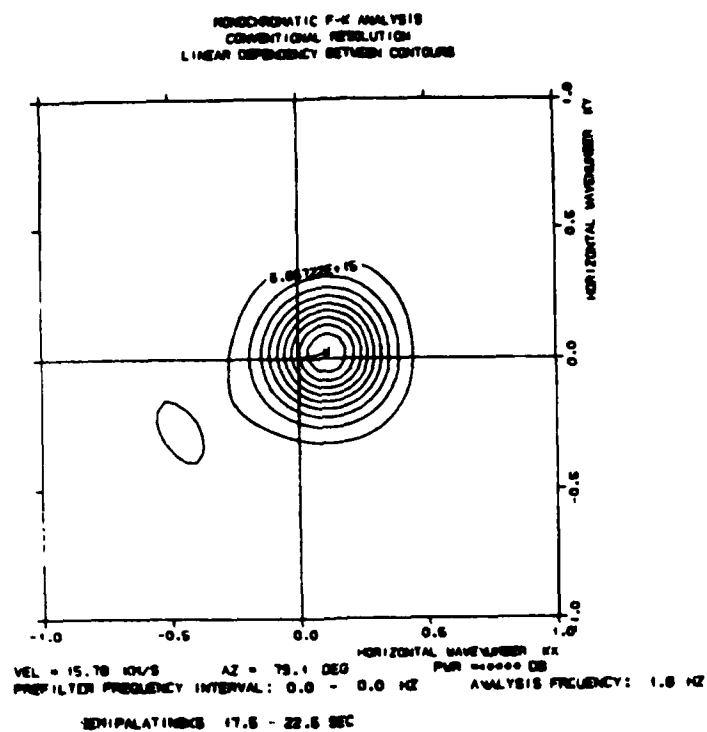
Figure 19.   As for Figure 18, but for Semipalatinsk, April 25.
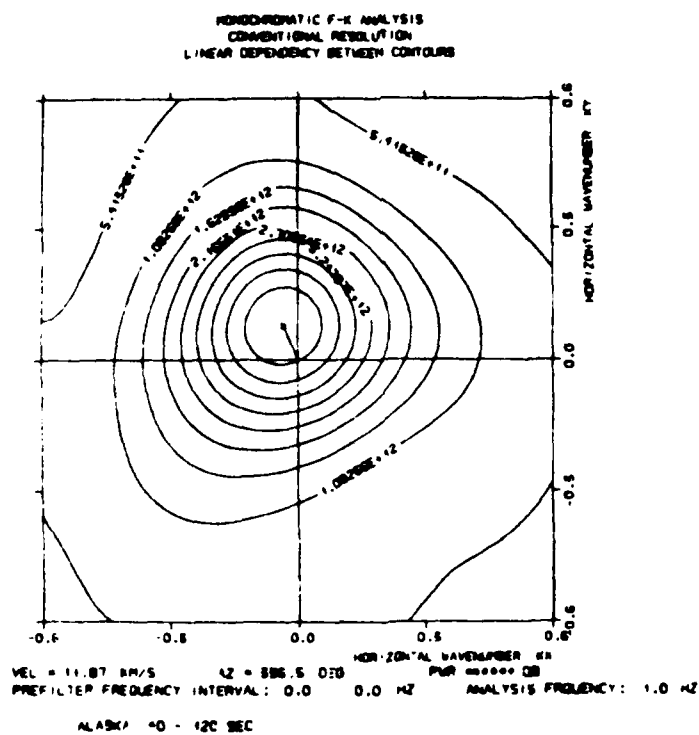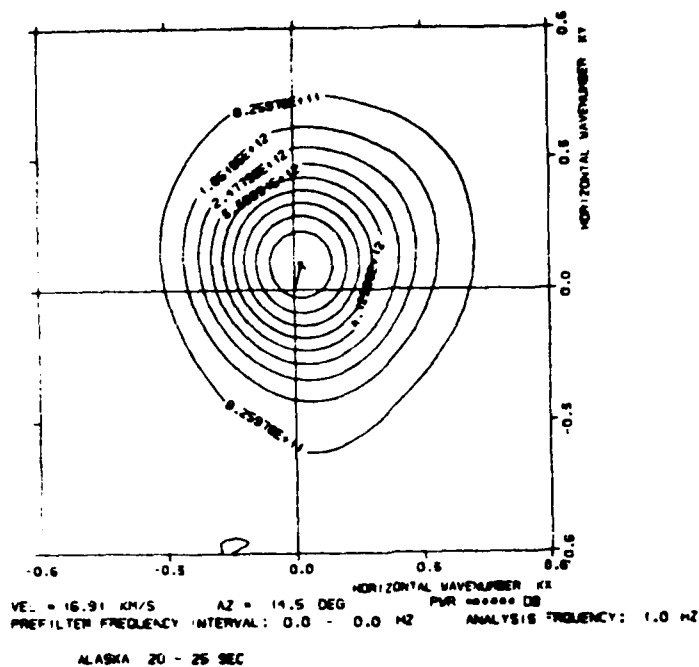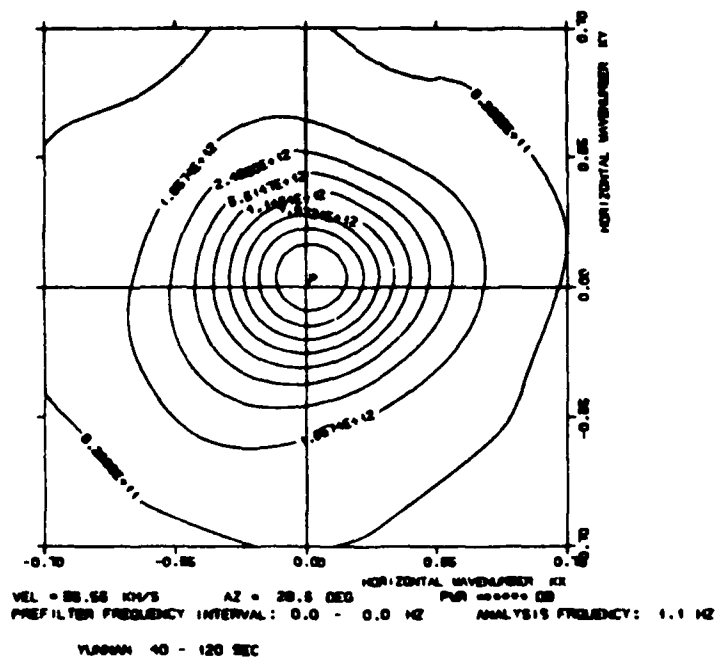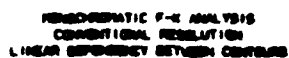
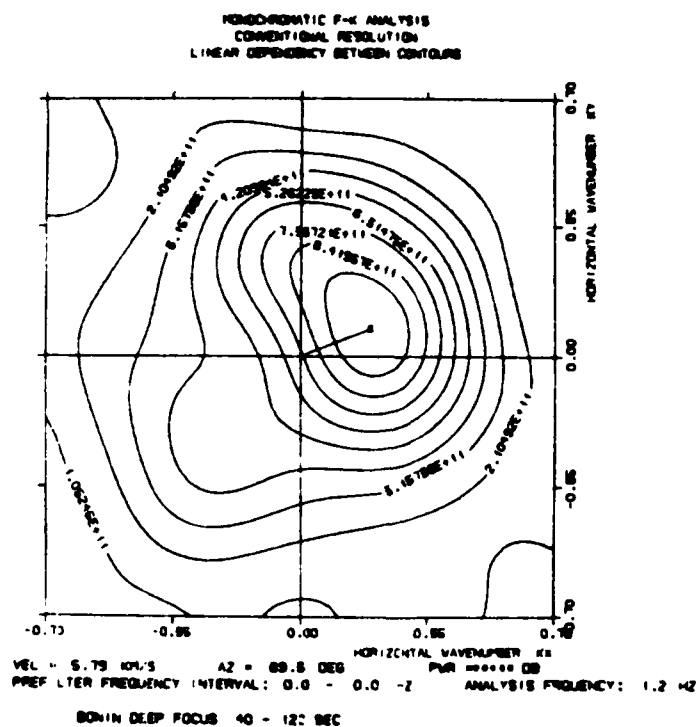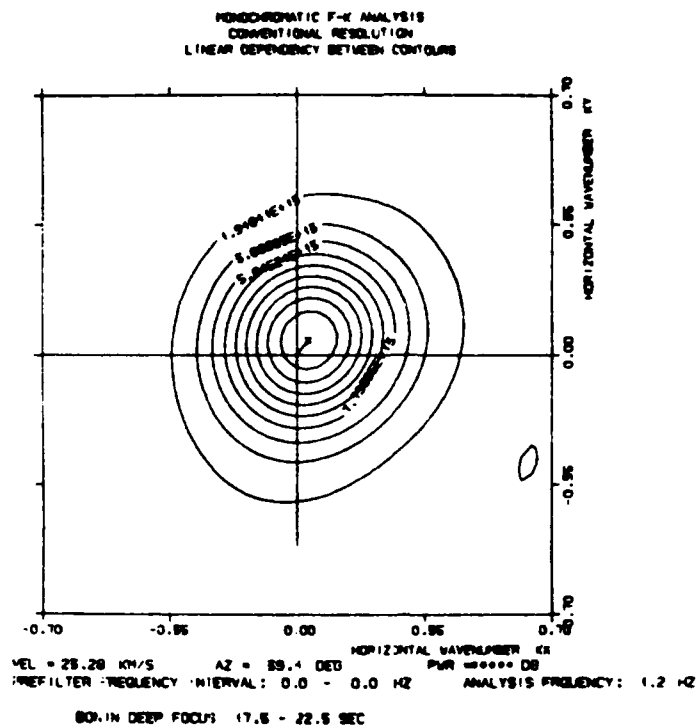Figure 20. As for Figure 18, but for Alaska, March 9.

Figure 21.   As for Figure 18, but for Yunnan, April 18.

Figure 22. As for Figure 18, but for Bonin, November 17, 1984.
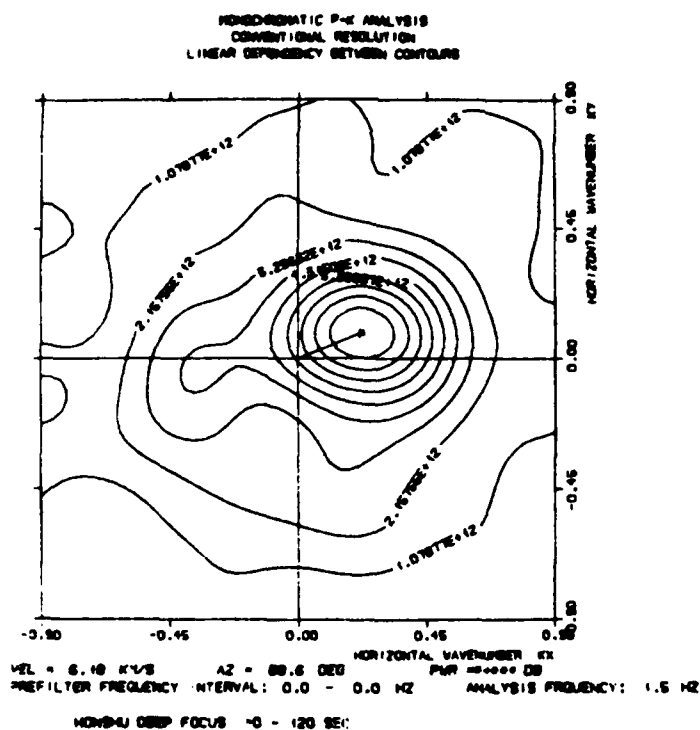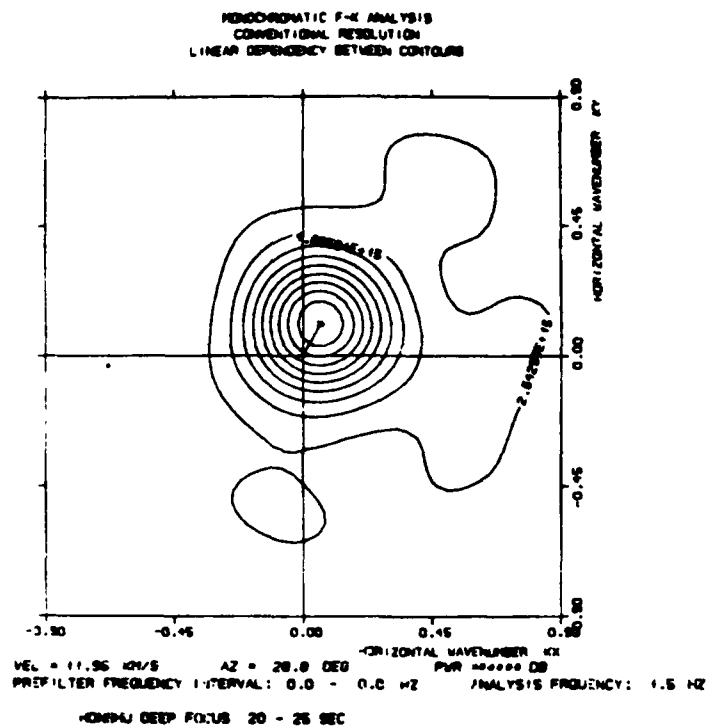
Figure 23. As for Figure 18, but for Honshu, April 10.

SEMIPALATINSK   1.8 HZ   15 - 20 SEC

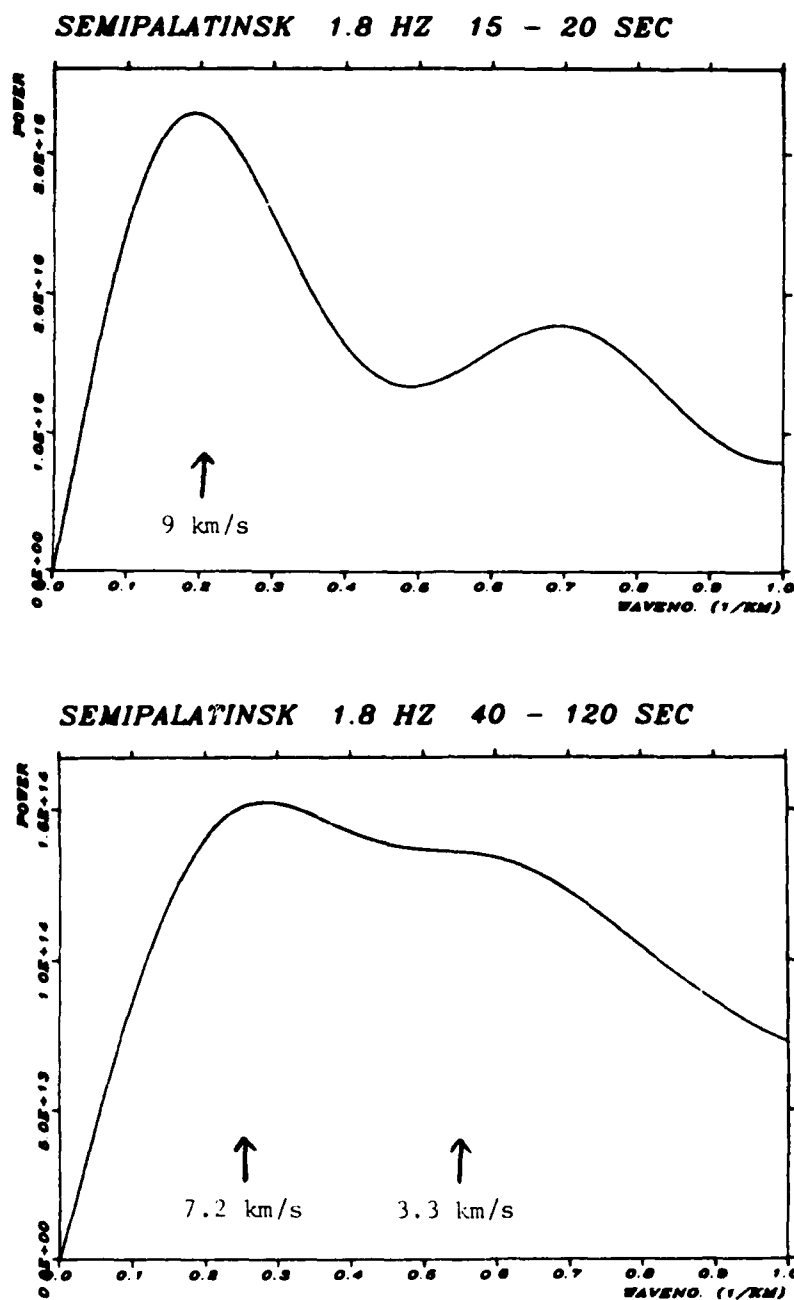SEMIPALATINSK   1.8 HZ   40 - 120 SEC

Figure 24.   Wavenumber spectra, Semipalatinsk, February 10.   The
frequency and time interval are written above each plot;
for times see Figure 16a.   Wavenumber is defined by
equation (23) and is related to the apparent velocity
by equation (24); selected apparent velocities are
indicated.   Power is in (bits)^2.   See text for discussion.

SEMIPALATINSK3   1.8 HZ   15 – 20 SEC

9 km/s

SEMIPALATINSK3   1.8 HZ   40 – 120 SEC

7.2 km/s   3.3 km/s
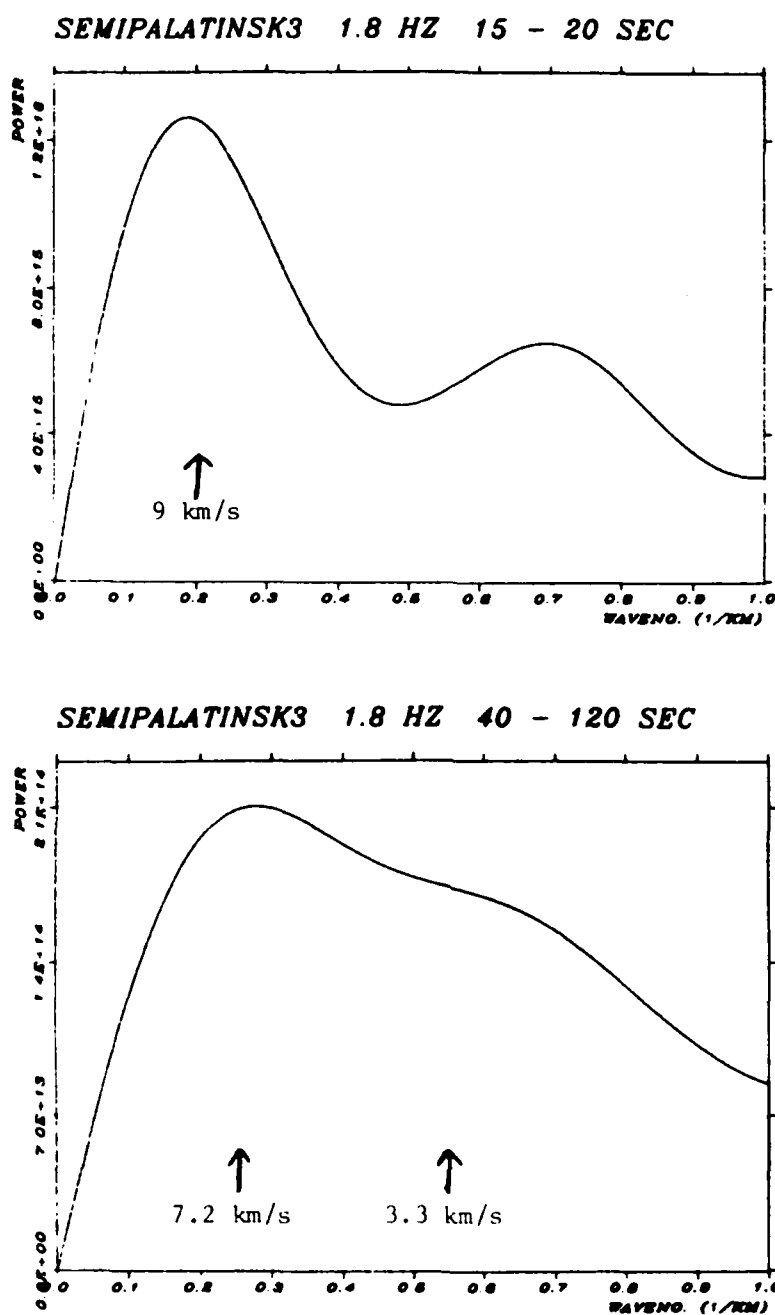
Figure 25.   As for Figure 24, but for Semipalatinsk, April 25.
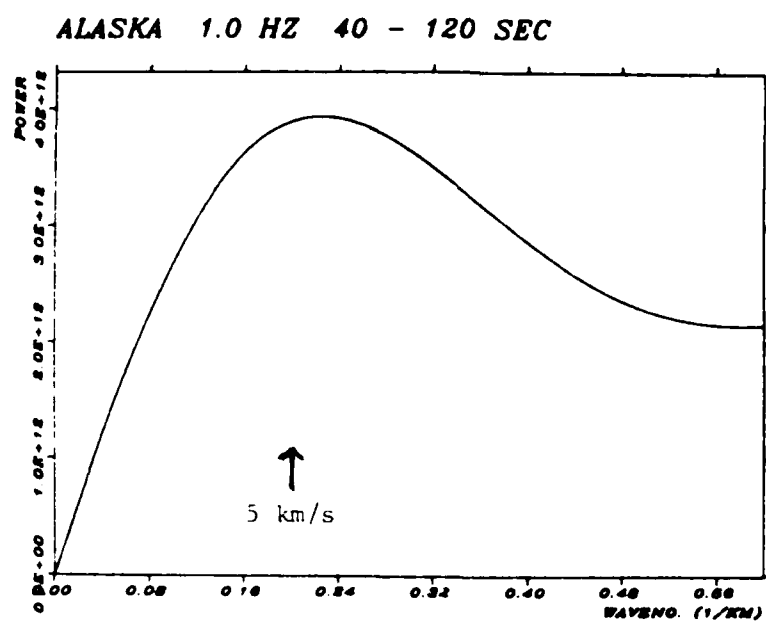
ALASKA 1.0 HZ 20 - 25 SEC

ALASKA 1.0 HZ 40 - 120 SEC
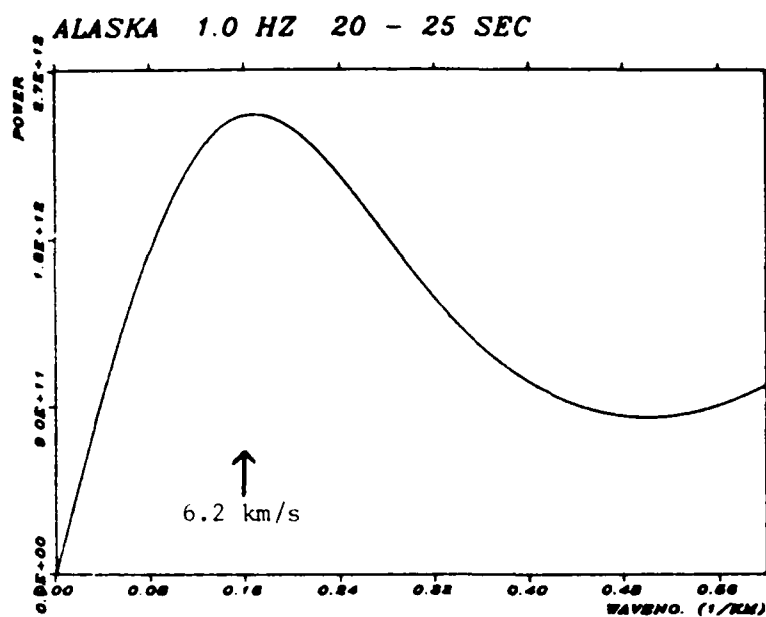
Figure 26. As for Figure 24, but for Alaska, March 9.

YUNNAN 1.1 HZ 20 – 25 SEC
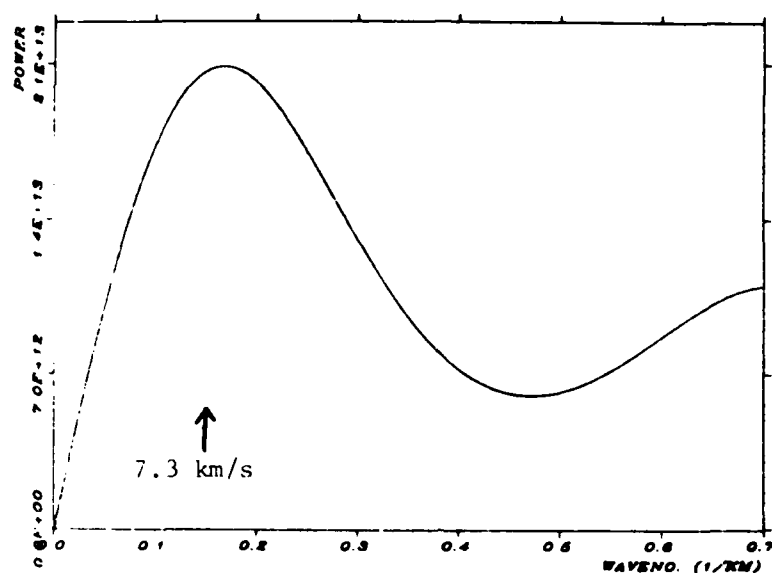
YUNNAN 1.1 HZ 40 – 120 SEC
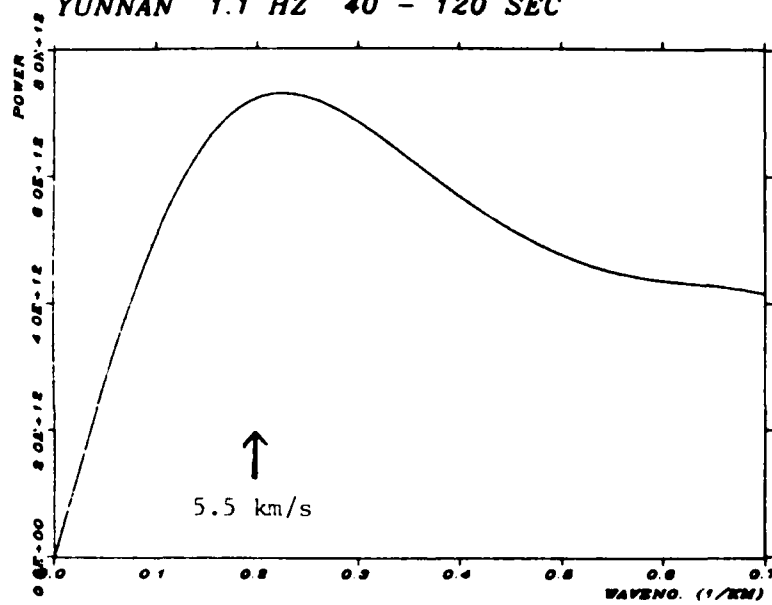
Figure 27. As for Figure 24, but for Yunnan, April 18.

BONIN DEEP FOCUS   1.2 HZ   15 – 20 SEC

BONIN DEEP FOCUS   1.2 HZ   40 – 120 SEC
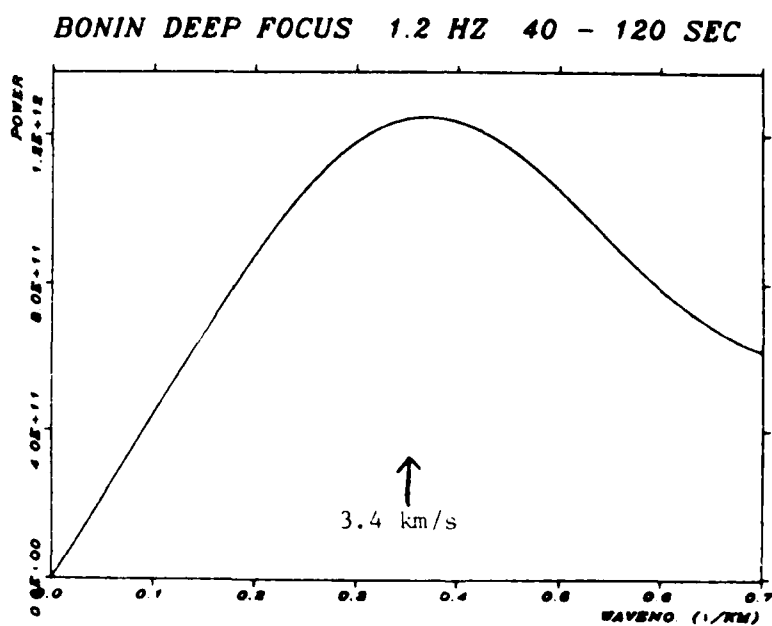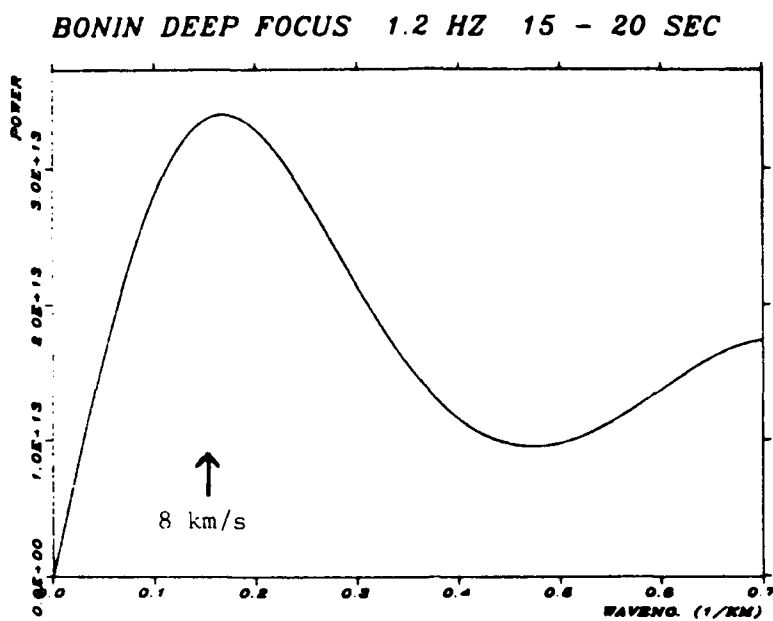
Figure 28.   As for Figure 24, but for Bonin, November 17, 1984.

HONSHU DEEP FOCUS   1.5 HZ   20 – 25 SEC

HONSHU DEEP FOCUS   1.5 HZ   40 – 120 SEC
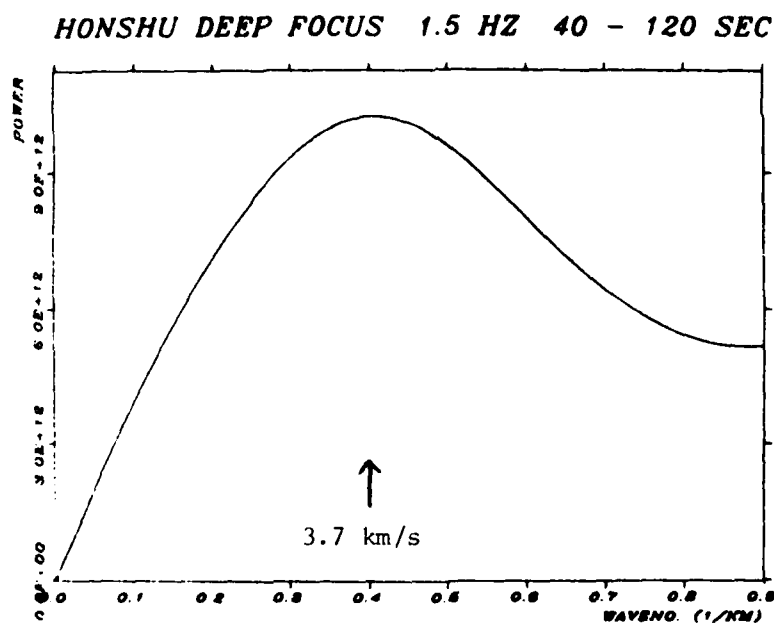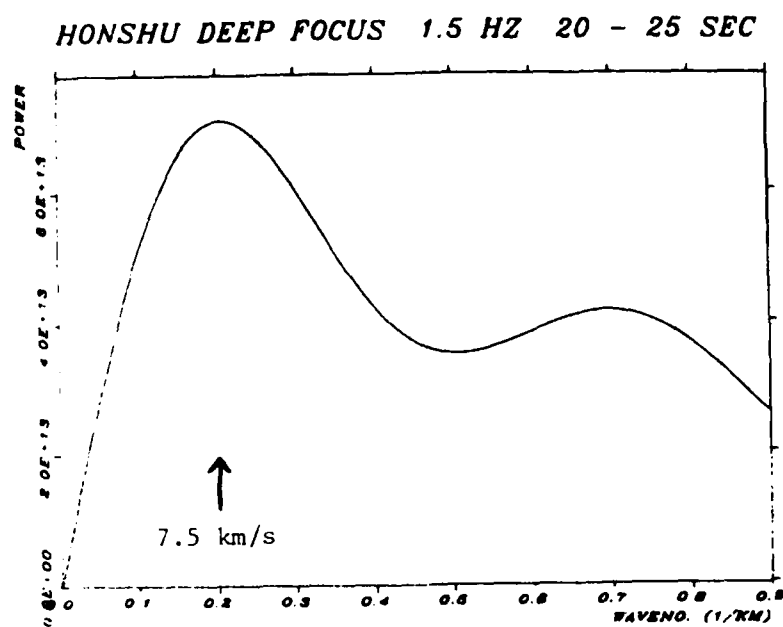
Figure 29.   As for Figure 24, but for Honshu, April 10.

wavenumber spectra for a window around first P and an average for the coda. It will be noted that the combination of finite resolution due to array aperture and the tendency of the wavenumber spectrum to increase with increasing wavenumber tends to bias the peaks towards higher wave-numbers (lower apparent velocity), especially at low wavenumbers and low frequencies (1 Hz). This will be discussed further in the next section.

DISCUSSION

Test of the Model

The three features of the model to be tested were: does scattering

occur in the crust near the receiver and near the source (if it is in

the crust), what is the nature of the scattered waves, and is the

scattering single or multiple. The first feature seems to be unambigu-

ously confirmed, especially by the wavenumber spectra shown in Figures

24-29. Whilst there is some bias in the apparent velocities, for

reasons discussed in the last section, this bias may be at least par-

tially assessed by comparing the first P windows of corresponding events

in Figures 18-23 (f-k spectrum) and Figures 24-29. Examining the two

deep-focus events (Figures 28 and 29), there is clearly a shift of

energy from low wavenumbers (high apparent velocity) in first P to high

wavenumbers (low apparent velocities) in the coda. These low apparent

velocities can only represent waves scattered in the crust near the

receiver; there seems to be little energy coming from near the source on

high apparent velocity paths, as the model predicts for these non-

crustal events. The explosions (Figures 24 and 25) retain the low

wavenumber, high apparent velocity energy seen in first P in their

codas, as noted by Greenfield (1971), but add to it a high wavenumber,

low apparent velocity, like that seen in the deep focus events. Under

the model the low wavenumber, high apparent phase velocity component is

due to scattering in the crust near the source, while the high wave-

number, low phase velocity component is due to scattering in the crust

near the receiver, as was the case for the deep focus events. For these

two explosions, approximately equal amounts of each component are seen. The two shallow earthquakes (Figures 25 and 26) show a situation in which the low wavenumber, high apparent velocity component dominates, even in the coda, although some spread of energy can be seen into the high wavenumber, low apparent velocity area compared to the first P. This indicates most scattering that produces the coda occurs near the source.

Further identification of the place of scattering of the high apparent velocity component, as well as the wave types involved, can be carried out by comparing the different types of events. The high wavenumber, low apparent velocity component has the typical phase velocities (3.5-4.5 km/sec) of Lg, or trapped crustal shear waves. Fits of equations (15) and (17) also indicate that Lg is important in the coda, as opposed to body waves, as discussed earlier. The situation near the source may be elucidated by noting that the deep focus events at NORESS have no near-source component, whereas the crustal events do, indicating a scattering of crustal phases to teleseismic P, and noting that the crustal earthquakes show much more near-source scattering than the explosions, indicating that Lg or possibly shear waves are involved, since an earthquake would produce more energy in these phases than an explosion. This difference is so dramatic that it may also be seen in the coda power fits for $\log_{10}G$ given in Tables 5 and 6. The crustal earthquakes all have much larger values of G (i.e., larger coda relative to first P) than other events at the same frequency. This is readily understandable in terms of equation (16), since (A_L/A_{po}) is large for a

crustal earthquake. Further, the depths of the crustal earthquakes are sufficiently deep that a phase like Lg must be involved, not Rayleigh waves as suggested by Greenfield (1971) since they will not be significantly excited at the frequencies involved. It will be noted that there does not seem to be any significant difference between the deep focus and explosion values of G, but this is because of the relatively large errors, ± 0.3 in $\log_{10}G$ or about a factor of 2. Comparing Figures 24 and 25 to Figures 28 and 29, this is about what would be expected for the difference.

One feature seen in Figures 22 and 23 is the possible importance of forward scattering of teleseismic P to Lg near the receiver. Since the events shown are both deep focus, this should be the dominant mode of scattering, and the coda peak lies in the same quadrant as the first P peak. In both cases, however, the quadrant is the northeast quadrant, and it is possible that there are simply more scatterers in this quadrant. Figures 18-21 demonstrate the importance of the high apparent velocity component of the coda coming from the source region (allowing for the finite resolution of the array) in the crustal events.

On the question of single as opposed to multiple scattering, it appears that multiple scattering is probably important. Even condition (19) for single scattering often fails, using the results quoted in Tables 5 and 6. Since G_a is ~ 0.005 km^{-1} at all frequencies, condition (20) implies, using $\nu = 4$ km/sec, that multiple scattering should be important for times longer than about 50 sec after first P onset, i.e., over most of the time interval examined. Whilst this calls into question the theoretical development leading to (15), nonetheless the

simple two-parameter model in (15) seems to fit the data well and may be a useful empirical formula. Similar results were found by Dainty et al. (1984) for the local coda. The finding that G_a is approximately constant with frequency is typical of high frequency scattering attenuation (Dainty, 1981, 1984; Dainty et al., 1984), although absorption band models can produce a similar effect (Bache, 1985).

In summary, the NORESS array studies strongly confirm the importance of scattering in the crust near the receiver and near the source if the source is in the crust for teleseismic coda in the time span 20-200 sec after first P; other contributions to the coda, such as PP (King et al., 1975), do not appear to be as important. There is strong evidence that trapped shear or Lg type phases are involved through Lg to teleseismic P scattering near the source and teleseismic P to Lg scattering near the receiver. Multiple scattering is probably occurring in the coda.

Implications for Yield Estimation and Discrimination

A basic purpose of this research was to understand the nature of the teleseismic P coda. Some comments may be made concerning the implications of the results for the yield estimation and discrimination problems. In yield estimation, the principal application has been to find a coda magnitude (Baumgardt, 1983; Bullitt and Cormier, 1984; Ringdal, 1983), since there is some indication that such a magnitude is less variable than conventional magnitudes. This study indicates that the stability of such magnitudes is probably because the scattered waves are regionally averaged over regions ~500 km in radius around the source

and receiver. The differences in regional crustal structure are impor-
tant, but focussing-defocussing by structures close to the shot and
receiver are probably not. An example of this is the lack of differ-
ences observed for the various presumed explosions at Semipalatinsk, the
similarity between NTS events studied and the similarity between deep
focus events. Equation (15) could be a basis for a coda magnitude
scale—it may be rewritten as

$$A_c(f,t) = A_o(f) \exp[-\pi ft/Q] \qquad (26)$$

where the A's are Fourier amplitudes in a prescribed window moved down
the seismogram. $A_o(f)$ would be the amplitude used in the magnitude
scale, which would apply only to explosions, since shallow earthquakes
have variable coda excitation near the source. The method would be
useful for large explosions, where the signal-to-noise ratio is good.

A further possibility would be the extraction of the coda due to
scattering near the source, by some analysis such as that shown in
Figures 24 and 25, where the low wavenumber (high apparent velocity)
component is coda from the near-source region. At the moment, long
averages such as those shown in Figures 24 and 25 appear to be necessary
to get good results—the short five-minute windows that are averaged to
obtain Figures 24 and 25 are very variable. This option and its uses
will be discussed further in the next section.

Another possibility that has arisen in this work is the use of P
coda as a discriminant for crustal earthquakes as opposed to underground
explosions through the apparent side-scattering turbidity G. All of the

crustal earthquakes in Tables 5 and 6 have higher values of G than the

explosions, indicating higher coda amplitude relative to first P.

A particularly dramatic example is the March 20, 1976, event near

Semipalatinsk (Figure 5) (Pooley et al., 1983). Seismograms from this

event received at NORSAR are shown in Figure 30, and should be compared

to Figure 6—the difference in coda to P amplitude is obvious. Several

other examples are shown in Bennett et al. (1984)—in all cases, events

with large Lg have large P codas, reinforcing the association between Lg

and near-source coda scattering. Thus P coda amplitude compared to P

might be used as a discriminant when Lg is blocked by geologic barriers.

Further Work

The study reported here is only a reconnaissance study of what is

possible. More events should be examined, analysis methods should be

refined, and the results obtained here should be used to derive further

information of benefit to the seismic detection, discrimination, and

yield estimation problems.

In terms of more events, shallow events and intermediate events

should be examined using NORSAR data. The Kamchatka-Kurile-Japan-Bonin

subduction zone, the southeast Asia and Hindu Kush region, and the

Alaska-Aleutian region could all supply data for both types. It would

also be interesting to look at the western United States and the North

Atlantic Ridge for shallow events, in the first case because of the

proximity to NTS, in the second case to see if the oceanic crust

produces different effects than a continental crust (it should). For

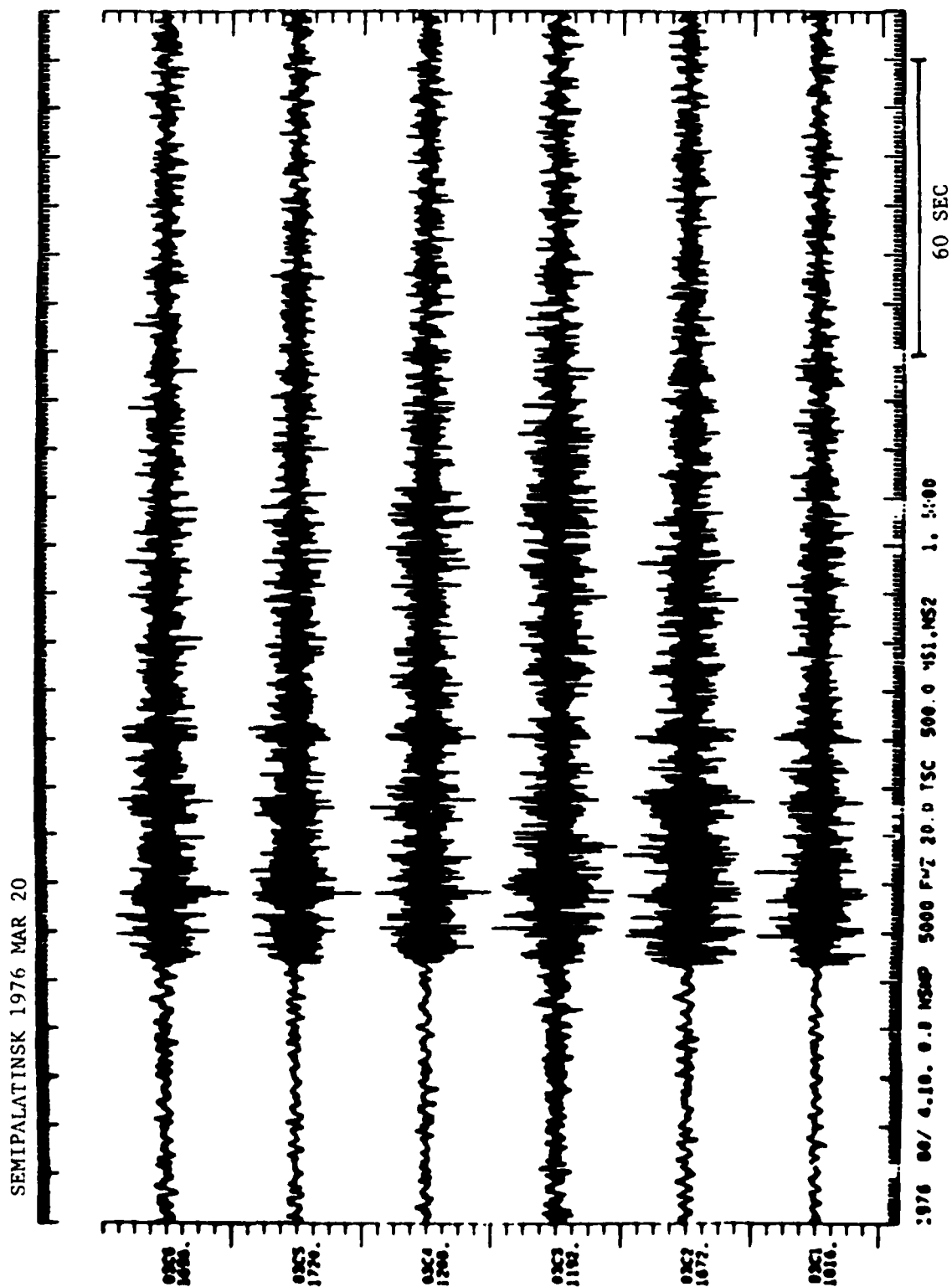NORESS, which has only been operating since late 1984, events in all

Figure 30. Semipalatinsk crustal earthquake (Pooley et al., 1983) recorded at 03C subarray, NORSAR.

these regions as well as events of the types used already should be analysed as they occur until a suitable data base is built up.

The analysis of NORESS data needs refinement. At present, all 25 verticals are used for single-frequency analysis. This has not been successful for frequencies above 2 Hz because of lack of coherence between traces, thus eliminating the use of local events, for example, and leading to problems with lack of resolution. The possibility of using only part of the array should be examined to improve coherence, or of using an average over a frequency band to improve stability and reliability. The problem of resolution and bias discussed with regard to the wavenumber (apparent velocity) analysis should be quantified.

The immediate focus of extensions of the method revolve around the question of whether a separation of the coda into source and receiver parts can be effected. Beamforming of unfiltered traces has not so far been effective because of the coherency problems. If the coda could be separated, an investigation of the characteristics of the source region, such as attenuation, would be possible. Another interesting question is the relationship between local measurements of coda and attenuation and teleseismic measurements. A measurement of coda attenuation at NORSAR gave $Q = 1500 \pm 300$ at 3.6 Hz, similar to estimates in Tables 5 and 6. This may be useful if measurements of local coda could be obtained near a test site.

ACKNOWLEDGMENTS

REFERENCES

Aki, K. (1969). Analysis of the seismic coda of local earthquakes as scattered waves, J. Geophys. Res., 74, 615-631.

Aki, K. (1980). Scattering and attenuation of shear waves in the lithosphere, J. Geophys. Res., 85, 6496-6504.

Aki, K., and B. Chouet (1975). Origin of coda waves: Source, attenuation, and scattering effects, J. Geophys. Res., 80, 3322-3342.

Aki, K., and P. Richards (1980). Quantitative Seismology Theory and Methods, Freeman.

Bache, T. (1985). Attenuation effects on body waves, Proceedings of a Workshop at Center for Seismic Studies.

Baumgardt, D. R. (1983). Teleseismic P-coda stability and coda-magnitude yield estimation (Abstract), 5th Annual DARPA Symposium on Seismic Detection, Analysis, Discrimination, and Yield Determination, p. 77.

Bennett, T. J., J. R. Murphy, D. G. Lambert, and J. M. Savino (1984). Discrimination with regional phases in the western United States and Eurasia, Basic Research in the VELA Program 1959-1984, DARPA, Santa Fe, New Mexico.

Bullitt, J. T., and V. F. Cormier (1984). The relative performance of m_b and alternative measures of elastic energy in estimating source size and explosion yield, Bull. Seismol. Soc. Amer., 74, 1863.

Dainty, A. M. (1981). A scattering model to explain seismic Q observations in the lithosphere between 1 and 30 Hz, Geophys. Res. Letters, 8, 1126-1128.

Dainty, A. M. (1984). High frequency acoustic backscattering and seismic attenuation, J. Geophys. Res., 89, 3172.

Dainty, A. M., and M. N. Toksöz (1981). Seismic codas on the Earth and the Moon: A comparison, Phys. Earth Planet. Interiors, 26, 250-260.

Dainty, A. M., R. M. Duckworth, and A. Tie (1984). Influence of scattering on Q in the lithosphere, Final Technical Report, Contract AFOSR-83-0037.

Greenfield, R. J. (1971). Short-period P-wave generation by Rayleigh wave scattering at Novaya Zemlaya, J. Geophys. Res., 76, 7988.

Ingate, S. F., E. S. Husebye, and A. Christofferson (1985). Regional arrays and optimum data processing schemes, Bull. Seismol. Soc. Amer. (in press).

King, D. W., R. A. W. Haddon, and E. S. Husebye (1975). Precursors to PP, Phys. Earth Planet. Interiors, 10, 103-127.

Mykkeltveit, S., and H. Bungum (1984). Procession of regional seismic events using data from small-aperture arrays, Bull. Seismol. Soc. Amer., 74, 2313-2333.

Mykkeltveit, S., and F. Ringdal (1981). Phase identification and event location at regional distance using small-aperture array data, Identification of Seismic Sources--Earthquake or Underground Explosion, E. S. Husebye and S. Mykkeltveit (eds.), Reidel, pp. 467-481.

Mykkeltveit, S., K. Astebol, D. J. Doorubos, and E. S. Husebye (1983). Seismic array configuration optimisation, Bull. Seismol. Soc. Amer., 73, 173-186.

Pooley, C. I., A. Douglas, and R. G. Pierce (1983). The seismic disturbance of 1976 March 20, East Kazakhstan: Earthquake or Explosion?, Geophys. J., 74, 621.

Ringdal, F. (1981). Automatic processing methods in the analysis of data from a global seismic network, Identification of Seismic Sources--Earthquake or Underground Explosion, E. S. Husebye and S. Mykkeltveit (eds.), Reidel, pp. 787-810

Ringdal, F. (1983). Magnitude from P-coda and Lg using NORSAR data, Fifth Annual DARPA Symposium on Seismic Detection, Analysis, Discrimination, and Yield Determination, p. 34.

Sato, H. (1977). Energy propagation including scattering effects single isotropic scattering approximation, J. Phys. Earth, 25, 27.

END
FILMED

5-86

DTIC